The Journal of Chemical Physics

Exploring chemical speciation at electrified interfaces using detailed continuum models

Cite as: J. Chem. Phys. **150**, 041725 (2019); https://doi.org/10.1063/1.5058159
Submitted: 17 September 2018 . Accepted: 29 November 2018 . Published Online: 04 January 2019

Artem Baskin, and David Prendergast

The Journal of Chemical Physics ARTICLE scitation.org/journal/jcp

Exploring chemical speciation at electrified interfaces using detailed continuum models

Cite as: J. Chem. Phys. 150, 041725 (2019); doi: 10.1063/1.5058159
Submitted: 17 September 2018 • Accepted: 29 November 2018 •
Published Online: 4 January 2019

Artem Baskin[a] and David Prendergast[b]

AFFILIATIONS

The Joint Center for Energy Storage Research, The Molecular Foundry, Lawrence Berkeley National Laboratory, Berkeley, California 94720, USA

[a]Electronic mail: abaskin@lbl.gov
[b]Electronic mail: dgprendergast@lbl.gov

ABSTRACT

We present a local free-energy functional-based generic continuum model for material interfaces with a specific emphasis on electrified solid/liquid interfaces. The model enables a description of multicomponent phases at interfaces and includes the effects of specific non-electrostatic interactions (specific adsorption), ion size disparity, and the explicit presence of neutral species. In addition to the optimization of electrostatic, non-electrostatic, and steric forces, the model can be easily modified to explore the effects of other channels for equilibration, including local chemical transformations driven by equilibrium constants and electrochemical reactions driven by the electrode potential. In this way, we show that, upon accounting for these effects, local speciation in the vicinity of the interface can be drastically different from what is expected from restricted models and minor species (from the bulk perspective) may become dominant due to the effects of local pH. We evaluate the ionic contribution to the surface tension at the interface and show how this could impact the structure of air/liquid interfaces. On the same footing, an attempt to describe electrochemical metal dissolution is made. The model allows estimates of the mutual population of newly produced ions depending on their charge and size and could be useful for interpretation of electrochemical and spectroscopic measurements if the dissolution involves different metal ions (species). With these advances, the proposed model may be used as an ingredient within a hybrid *ab initio*-continuum methodology to model biased interfaces.

I. INTRODUCTION

The advancement of energy harvesting and storage devices is a key requirement to support a growing portfolio of intermittent renewable sources of energy, electrified transportation, and complex power grid management as we strive for a truly sustainable society. A major stumbling block for much-needed advancement in nanofabrication for energy technologies is the lack of detailed knowledge of active material interfaces—a vital ingredient of any functional combination of two materials. Such functional interfaces usually combine contrasting components that are greatly affected by reduced dimensionality and spatial inhomogeneity. As a result, functional interfaces can demonstrate non-additive and emergent properties, distinct from the bulk properties of the comprising materials. Such functional modulation, in concert with the characteristic size scales of these interfacial regions, requires special means to understand, probe, and control interfaces at the molecular scale, which remains elusive, to date, for both theory and experiment.

This is particularly true for electrochemistry, for which the ultimate goal is to provide a mechanistic explanation of macroscopically observable behavior in terms of underlying principles and interfacial phenomenology at the microscopic level, including the energetics of elementary chemical acts and associated molecular structures at various conditions. Only recently, advances in experimental techniques, such as ambient pressure tender X-ray photoelectron spectroscopy (AP-trXPS)[1–3] and X-ray absorption spectroscopy in the

interface-sensitive electron yield mode (EY-XAS),[4] are enabling access to buried interfaces with elemental and chemical specificity. The interpretation of these experiments is notoriously difficult and, in the absence of pre-existing standards for comparison, should ideally be paired with reliable thermodynamic data on the interfacial molecular structures and their speciation. However, due to the ambiguities related to probing length scales of different techniques [e.g., surface enhanced IR versus Ambient Pressure X-ray Photoelectron Spectroscopy (APXPS)] and fundamental differences in protocols of measurements (spectroscopy versus conventional electrochemical techniques, e.g., voltammetry), the direct inferences from either spectroscopic data or electrochemical characterization (or even both) may not be conclusive, thus leading to uncertainties and a variety of models of interfacial composition that "fit" the observations. Accordingly, the benchmarking between theoretical models and experimentally inferred pictures of electrochemical interfaces will then be biased.

Likewise, the conflict between different theoretical approaches originates from the contention between macroscopic and microscopic descriptors used to model electrified solid/liquid interfaces. The macroscopic descriptors are based on equilibrium thermodynamics supplemented with classical continuum equations to account for the effects of joint charge and mass/heat transport.[5,6] The estimates of energetics and kinetics of relevant processes are then derived from the assumption of homogeneity of the contacting phases such that in thermodynamic cycles, the initial and end points belong to well-defined phases.[7–12] Thus, redox potentials ignore the interfacial inhomogeneity (e.g., the deformation of solvation spheres of ions and their partial desolvation at the interfaces) and may impair estimates of electrochemical stability of electrolytes. On the other hand, the connection between the Gibbs isotherm $-d\gamma = \sum_i \Gamma_i d\mu_i$ and the surface excess of components at electrified interfaces not only involves chemical potentials defined (typically) for ensembles of non-interacting particles $[\mu_i = \mu_{i0} + RT\log(c_i/c_0)]$ but also requires extra thermodynamic assumptions, related to the additivity of electrostatic and non-electrostatic forces.[13–17]

The fundamental problem in deriving microscopic descriptors of interfaces (e.g., molecular energy levels, surface speciation, etc.) is to realize atomistic simulations consistent with electrochemical conditions that would guarantee the thermodynamic stability of interfaces while including both the electronic and ionic degrees of freedom. This can only be realized when the molecular structure of the interface is consistent with the targeted external conditions (e.g., voltage and concentration). However, a mismatch of several orders of magnitude between the time and space scales of different processes puts severe limits on the feasibility of *ab initio* molecular dynamics (AIMD) protocols. Electron transfer (ET) events occur on attosecond to femtosecond time scales across tenths of Å. By contrast, solvent dipolar relaxation requires tens to hundreds of picoseconds (e.g., for water, the dipolar relaxation time is ~10 ps, while for a bulkier aprotic solvent, diglyme, it is already ~300 ps). Ion diffusion/migration times may be on the order of nanoseconds across characteristic distances of up to tens of nanometers. On the other hand, the description of the Faradaic regime would require accounting for charge transfer events that are extremely rare at the atomistic scale. A typical current density of 10 mA/cm^2 implies only 6.2×10^{-7} charge transfer events per 1 ns and 1 nm^2. Therefore, the observation of bias driven electrochemical reactions during regular AIMD protocols is clearly beyond computational feasibility. Moreover, the implications from the observed reactivity of an electrolyte near the electrode surface induced by the charge transfer are fraught with conceptual difficulties. For example, the rates of electrochemical reactions simulated in limited *ab initio* setups could be severely overestimated and result from highly non-equilibrium initial molecular configurations. Thus, these simultaneous length and time scale requirements are already at odds with the current computational feasibility for first-principles calculations and require serious re-thinking of the meaning of a computational experiment in a "single-molecule near the electrode surface" mode. Furthermore, within standard AIMD models of condensed phases as finite simulations cells under periodic boundary conditions, the technical requirement of global neutrality places additional constraints on realizing sensible simulations of the electric double layer (EDL). For example, a cell with dimensions 10 Å × 150 Å^2 contains only one ion pair per ~50 water molecules if the bulk concentration of a monovalent binary solution is n_b = 1M, meaning that the smallest surface charge density σ_{min} = 10.7 μC/cm^2 = 1e/150 Å^2 realizable within this simulation cell corresponds to retaining only a single charged species (cations or anions alone) within the AIMD, which is hardly an appropriate model of the EDL.

Two major strategies have been developed to model electrochemical interfaces within the framework of (AI)MD. In the *const*-q_e approach,[18–28] the total charge and/or the surface excess charge as well as the number of species are fixed. These studies focus on the molecular optimization and relative free energies of reaction intermediates. Depending on the implementation scheme, the computational electrode potential is converted into a physical scale either through a computational hydrogen electrode[29] or the absolute position of a standard hydrogen electrode.[30] Due to insufficient accounting for the electrolyte response and unrealistic molecular configurations (see below) at the interface, this approach leads to large uncertainties in electrode potentials and potential of zero charges (PZC) as well as the EDL capacitances. Interestingly, attempts to evaluate the electrolyte stability within this approach invoke the ensemble average positions of HOMO and LUMO orbitals of the electrolyte referred to the Fermi level of a metal electrode[31] as opposed to the thermodynamic recipe that invokes the redox potentials. Direct studies of the stability of electrode/electrolyte interfaces usually rely on simple charge analysis[32,33] performed at each MD step. In these cases, extra caution is required to avoid strongly non-equilibrium configurations and the method to convert surface

charge densities to electrode potentials at which electrolyte decomposition occurs remains ambiguous. When applied to intercalation cathode materials,[34] this scheme allows easy referencing to the metal redox potential (e.g., Li^+/Li) through the lattice formation energy. However, this approach requires the chemical equilibrium $\mu_e = \mu_{Li^+}$[35–37] leaving the electrode material neutral which complicates the simulation of processes at the interface.

In principle, the ideal description of electrochemical interfaces should be performed at constant electrode potential (*const*-μ_e) allowing the electronic charge to fluctuate by flowing in or out in response to the electrolyte behavior, thus enabling the modeling of both the capacitive and Faradaic regimes. There are a variety of potentiostat schemes, depending on the connection to the reservoir of electrons (implicit or explicit presence of an electrode[38]), methods for energy minimization,[39] referencing of the electrode potential,[40,41] half- or full-cell setups,[42] and what portion of the electrolyte is modeled explicitly.[43] The common problem for the *const*-μ_e approach is related to finite size effects. According to the fluctuation-dissipation theorem,[44] the variance of the surface charge density scales with the surface area S as $\sqrt{\langle\sigma^2\rangle} = \sqrt{C_{dif} k_B T/S}$. For a computationally tractable supercell, with S = 100 Å^2 and a capacitance of 50 μF/cm^2, $\sqrt{\langle\sigma^2\rangle} = 4.5\,\mu$C/cm^2 ($2.8 \times 10^{-3} e/$Å^2). The magnitude of thermal fluctuations of the electronic energy levels to be expected depends on the molecular structure of the EDL, but, with a limited number of screening species, these fluctuations can easily exceed thermal energies (k_BT). Likewise, the standard deviation of the electrode potential caused by the thermal fluctuations of a polar solvent in the *const*-q_e regime[45] in a computationally tractable supercell can be enough to (de-)populate molecular orbitals of species expected to be electrochemically stable near the electrode surface. For example, a supercell volume 10 Å × 100 Å^2 containing 32 water molecules can exhibit potential fluctuations of $\sqrt{\langle\varphi^2\rangle} = 0.51$ V, i.e., inducing fluctuations in the local electronic chemical potential of several k_BT above (or below) the Fermi level (a factor of ~20 at room temperature), which could easily result in artificial electrochemical activity.

Issues related to stability can be aggravated when the *const*-μ_e approach is applied intentionally to observe the electrochemical/catalytic reactions. Locally, ET events followed by rupture of chemical bonds or metal deposition/dissolution instantaneously give rise to highly non-equilibrium configurations since the rate at which the electron population is restored is much faster than time scales associated with the slow motion of the electrolyte. Therefore, to restore the constant electrochemical potential of the lost species, this scheme should be ideally paired with the approach that would provide the constant chemical potential of ions (*const*-μ_{ions}).[46] However, adding or removing even one electron or proton for realistic AIMD unit cells may cause a drastic change in the electrode potential by ±1.0 V.[22] Moreover, it remains generally unclear how to reconcile a microscopic picture where a single ET event may cause a cascade of reactions, in contrast to the macroscopic thermodynamic picture, where these reactions subside or are suppressed.

We are confronted again by the contention between the thermodynamically motivated equilibrium at the interface and its microscopic realization in AIMD simulations. For example, in the presence of specifically adsorbing ions, the equilibrium surface population (which defines the surface dipole and to a great extent the energetics of ET) is usually derived from equalizing the electrochemical potentials of species in the bulk and at the interface $\tilde{\mu}_{i,bulk} = \tilde{\mu}_{i,int} + \Phi(z)$, where $\Phi(z)$ is the single particle free energy of adsorption averaged over the (x, y)-plane in the infinitely dilute limit (suitable for *ab initio* simulations which may be limited to describing a single solute). This leads to a well-known expression for the equilibrium interfacial concentration profile

$$\rho_{i,int}(z) = \rho_{i,bulk} \exp\left(-\frac{\Phi(z) + e\varphi(z)}{k_B T}\right). \quad (1)$$

However, even for the case when the solvent induced surface dipole or the electrode surface charge density (e.g., neutral electrode) could be disregarded, the interfacial population for a solution of finite concentration, given by Eq. (1), will be erroneous since it ignores interparticle interactions. Moreover, the conditions at which the concept of the average electrostatic potential $\varphi(z)$ is even applicable go beyond the infinitely dilute limit when and only when $\Phi(z)$ is well defined. One might assume that this problem could be resolved by using the single particle adsorption potential $\Phi(z)$ calculated (e.g., with AIMD methods) for the solution of the finite concentration. However, this approach inherently requires the thermodynamic equilibration between the interface and the bulk solution such that the electrode surface should be populated with some (if any) surface excess of electrolyte species. The practical realization of this state in AIMD simulations is by no means a trivial task. We may easily run into a situation when all the adsorbates populate the interface leaving behind no species in the bulk. In the system with finite number of adsorbates in the simulation cell, their electrochemical potential across the cell will not be constant meaning that equilibrium is not yet reached. Moreover, we can bring up another fundamental argument against this approach. Even if we succeed and realize the true equilibrium in the inhomogeneous system, the single particle adsorption potential $\Phi(z)$ has no value anymore since at this state there should be no free energy benefits for the particle to be at the interface versus the bulk. Therefore, $\Phi(z)$, obtained in such a way, cannot be used to define the surface population [e.g., in Eq. (1)] since it already requires the knowledge about the equilibrium population at the interface—the information that we actually seek.

This analysis shows that even the computationally extensive AIMD free energy sampling could be misused to provide the information about the equilibrium molecular configuration at the interface. Instead, single particle free energies should be properly paired with more advanced models of the chemical potential which include interparticle interactions either

at the mean-field level or directly through pair correlation functions.

Another problem for AIMD protocols is that it is generally unclear what the parameters of the AIMD unit cells (size/simulation times, boundary conditions, and number of species) should be to provide meaningful modeling of both the static properties of electrochemical interfaces and the dynamics of electrochemical reactions in a unified and realistic framework. Further theoretical work in developing hybrid approaches[47,48] is needed.

Continuum models (CMs) represent an alternative approach to model interfaces that is intermediate between the conventional thermodynamics and AIMD. During the last few decades, considerable progress has been made using a variety of methods, such as the Wertheim-Lovett-Mou-Buff integral equation,[49,50] modified Poisson-Boltzmann equation (MPBE) mixed with lattice cite models,[22,51–58] hybrid theories based on the Ornstein-Zernike equation, and the reference interaction site model (RISM).[59,60] A common basis for these approaches is classical density functional theory (CDFT)[61–64] which states the existence of a universal functional, $\Omega[\rho]$, of a single-particle number density, ρ, at a fixed external potential V^{ext} whose minimization

$$\left.\frac{\delta\Omega[\rho]}{\delta\rho}\right|_{\rho=\rho^*} = 0 \tag{2}$$

gives the physically meaningful density ρ^* at which the functional yields the corresponding grand canonical potential Ω. If we can derive the self-consistent, one-body, direct correlation function, defined as a functional derivative of the intrinsic excess free energy $c^{(1)}(\rho) = -\frac{1}{k_B T}\frac{\delta\mathcal{F}^{exc}}{\delta\rho}$, which includes all additional interactions beyond the ideal gas, then the equilibrium density profile can be defined as

$$\rho = \exp\left(\frac{\mu - V^{ext}}{k_B T} + c^{(1)}(\rho)\right). \tag{3}$$

Accordingly, there is a hierarchy of approximations of $\mathcal{F}^{exc}[\rho]$ as well as strategies for solving Eq. (3) that encompass models of hard sphere[65] and Lennard-Jones liquids[66] and extensions to a variety of models of multicomponent ionic solutions.[67] CDFT successfully explains a range of phenomena including phase transitions in hard sphere liquids, layering of solvents near immovable walls of various geometries and topologies, wetting conditions, etc. Typical benchmarks for CDFT models are provided by a limited number of known exact results (e.g., the contact density theorem[68]) and direct comparison with Monte Carlo (MC) or MD simulations, where ensembles of model particles are explored. Despite good agreement achieved for model systems, any attempts to go beyond mono-atomic liquefied noble gases face fundamental challenges. Not only that the attempts to incorporate realistic interactions into the free energy functional lead to a loss of analytic elegance and tractability,[69,70] but the ultimate computational cost may become comparable to explicit MC/MD simulations. Furthermore, given that reliable force-field parameters may not be available for a given system, the only solution then is to return to AIMD. In fact, it is well known that the local density mean-field approximation (LDA-MF), which is a basis for the Gouy-Chapmen-Stern model, cannot even capture the density oscillations near charged particles or walls, and, in order to describe the double layer in equilibrium, one needs to use non-local functionals in various weighted density approximations (WDA)[71] which requires solving non-linear integro-differential equations. Nevertheless, CDFT remains the only appropriate tool for exploring long-ranged intermolecular correlations and associated collective phenomena.

Current applications of CDFT to electrochemistry, which might be considered straightforward, have been limited to the capacitive regime of the EDL[72] with a special emphasis on the ensemble average structure of the EDL and the associated differential capacitance. In the majority of such studies, the connection to real electrochemical materials and their microscopic descriptors, such as the electrochemical stability, HOMO–LUMO gap, etc., is not well defined. This can result in unphysical voltage ranges for the differential capacitance, possibly exceeding 6 V,[73,74] which is well beyond the stability limits for many electrolytes. Moreover, many refinements, whose description requires advanced Green's function techniques,[75,76] able to provide additional insights into the structure of the EDL, may be less relevant to electrochemical applications, since they neglect all but electrostatics factors. Besides contributions from the self-energy of image charges, it remains to be seen what additional role can be played by specific adsorption and steric factors.

In this context, the joint DFT (JDFT) approach[39,77–79] represents a far more advanced methodology: with (1) more elaborate models of ion solvation and the non-linear dielectric response of the electrolyte in contact with the electrode and (2) a quantum-mechanical treatment of the electronic degrees of freedom within the electrode. In this way, JDFT combines the virtues of *ab inito* methods and continuum models, although the current implementations retain the same generic drawbacks of all continuum models—the absence of ET and specific adsorption.

Therefore, if the final goal is to develop a hybrid AIMD-continuum protocol that is focused on the atomistic understanding of electrochemical processes at interfaces without compromising their thermodynamic stability, it might be much more practical to reduce the complexity of the CDFT continuum models emphasizing aspects that are more relevant to electrochemistry. In fact, many aspects of the capacitive regime were successfully studied with adapted phenomenological free-energy functionals giving rise to mean-field models[22,55,80] that are based on the MPBE[57]

$$[\nabla\cdot\varepsilon(\vec{r})\nabla - \Im]\varphi(\vec{r}) = 0 \tag{4}$$

with a spatially dependent dielectric function $\varepsilon(\vec{r})$ that indirectly depends on the electric field or the charge density of the ions.[81–83] Here, $\Im$ includes the steric effects of the finite size of the ions and other factors relevant for the system. In this way, the anatomy of the EDL was disclosed and the shape

of the differential capacitance curves was discussed in great detail.[56,73,84,85] Dielectric and ionic nonlinearity, lattice saturation, and image charge effects are listed among factors that affect the shape of the differential capacitance curves. The ion size disparity was extensively studied in various theoretical frameworks. The difference in parameters of the Helmholtz compact layers for cations and anions was shown alone to induce the asymmetry in capacitance[86,87] without introducing explicitly the sizes of ions. On the other hand, the asymmetric Wicke-Eigen model[88] or advance CDFT primitive models[89,90] gives qualitatively similar results in this respect. This shows that the key features of the electrochemistry relevant quantities can be obtained with drastically different levels of theory.

Being motivated by a long term goal of developing a hybrid AIMD-CM protocol suitable for studies of electrochemical reactions in thermodynamically stable realistic conditions, in this work, we propose a simple continuum model of multicomponent electrolytes with ions of unequal sizes that captures the effects of specific adsorption and the local chemical equilibrium in addition to the equilibration of Coulombic, non-electrostatic, and steric forces. With simple modifications and external inputs provided by AIMD simulations, the model allows getting electrolyte layering at the solid/liquid interfaces without introducing non-local functionals. The model can be easily applied to other types of interfaces including air/liquid and liquid/liquid interfaces. We also show its connection to other electrochemical observables, such as adsorption isotherms and the surface tension which allows quantitative studies of non-equilibrium molecular configurations. With properly tuned input parameters that can be obtained from AIMD simulations, the proposed advanced model may become a part of a self-consistent AIMD-CM methodology of studies of electrochemical interfaces.

II. THEORY

Our starting point is the LDA-MF grand canonical free-energy functional developed originally in the framework of the lattice gas model[51,52,91,92] which accounts for the Coulombic interactions between particles of finite size but neglects the core-core repulsion. Due to the debate of the authorship of this class of functionals, we will call it the Gouy-Chapman model with exclusion volume (GCEV). As such, this functional describes the restricted primitive model as defined in the CDFT classification. Upon introducing hard spheres through the excess entropic terms but keeping the point-like electrostatic interactions, this functional effectively accounts for the ion correlations due to the "interaction hole" created by hard core exclusion thus amounting to an approximation of the "Coulomb hole" by a totally different (i.e., non-Coulombic entropy driven) mechanism of exchange repulsion as opposed to the proper Hartree repulsion. This imbalance between the enthalpy and the entropy makes this functional well suited for the description of solutions of high salt concentrations at the expense of lower accuracy for low concentration solutions.[67] Moreover, this lattice-based model grossly underestimates steric effects in hard sphere liquids as compared to the Carnahan-Starling equation of state for monodisperse hard-sphere liquids.[56] Finally, since lattice models define volume fractions from the density only locally, these models, strictly speaking, are valid only for homogeneous density profiles. However, the MPBE derived from this functional provides (as we shall see) a very good description, as compared to other advanced local and non-local functionals, of differential capacitance, implying that the profile of the electrostatic potential at the electrode must be somewhat decoupled from the structure of the rest of the EDL.[72]

A. Ion-size disparity

Here, we extend the lattice gas model and propose a GCEV functional that includes the disparity in the size of ions and non-electrostatic interactions of particles with the flat electrode surface. For an electrolyte containing $\mathcal{N}$ species (including cations, anions, and neutral molecules) of charges ζ_X and effective sizes a_X, it reads

$$\Omega[\varphi(z);\rho_{1\cdots\mathcal{N}}(z)] = \sum_X^{\mathcal{N}} \left(\int dz \left(-\frac{\varepsilon(z)}{8\pi}|\nabla\varphi|^2 + \zeta_X e\varphi\rho_X + \Phi_X(z)\rho_X - \mu_X\rho_X \right) + \frac{k_BT}{a_X^3}\int dz\, a_X^3\rho_X \ln(a_X^3\rho_X) \right) + \frac{\mathcal{N}k_BT}{\sum_X a_X^3}\int dz \left(1-\sum_X^{\mathcal{N}} a_X^3\rho_X\right)\ln\left(1-\sum_X^{\mathcal{N}} a_X^3\rho_X\right). \tag{5}$$

The terms $\frac{k_BT}{a_X^3}\int dz\, a_X^3\rho_X \ln(a_X^3\rho_X)$ describe the free energy (translational entropy) of ideal gases and the functional form of the volume exclusion term we constructed heuristically to meet the key extreme cases. Specifically, it provides the continuous transition to both the Gouy-Chapman free energy functional and the original symmetric GCEV model in terms of the relationship $f(\rho_1,\rho_2,\ldots\rho_{\mathcal{N}}) = 0$ between density profiles of species (see below). The variation $\frac{\delta\Omega}{\delta\varphi} = 0$ and $\frac{\delta\Omega}{\delta\rho_{X'}} = 0$ gives the MPBE

$$\nabla\cdot\varepsilon(z)\nabla\varphi = -4\pi e\sum_{X'}\zeta_{X'}\rho_{X'}, \tag{6}$$

where X′ goes over the charged species and $\rho_{X'} = \rho_{X'}(\varphi, z)$, the so-called "polarization curves," cannot usually be expressed in an analytic form and the chemical potentials $\mu_{X'}$ guarantee that $\rho_{X'}$ converge to bulk concentrations n_{Xb} as $\varphi \to 0$ and the additional cationic/anionic potential profiles $\Phi_X(z) \to 0$ as $z \to \infty$. For a binary 1:1 electrolyte of ions with sizes a and b, despite the non-analyticity, $\rho_\pm$ in the absence of adsorption potentials $\Phi_\pm(z)$ are related through the simple "phase relationship"

$$\frac{\rho_+\rho_-}{n_b^2} = \left(\frac{1-a^3\rho_+ - b^3\rho_-}{1-(a^3+b^3)n_b}\right)^2 \tag{7}$$

which is valid irrespective of the boundary conditions and reduces in the symmetric case $a = b$ to the original relationship of the GCEV model[93] and to $\rho_+\rho_- = n_b^2$ of the Gouy-Chapman

model as $a, b \to 0$. The excluded solvent volume entropy term in Ω guarantees the upper bound of the concentration $\frac{1}{a^3}$ for cations and $\frac{1}{b^3}$ for anions. The numerical solutions of Eq. (6) were obtained from an adaptive shooting-like algorithm. The upper bound for the boundary conditions was set as $z = 20$ Å. The "polarization curves" $\rho_{X'}(\varphi)$ with explicit dependence on the electrostatic potential φ were obtained from the numerical solutions of the system of non-linear algebraic equations $\frac{\delta\Omega}{\delta\rho_{X'}} = 0$. In the presence of adsorption potentials, we developed a self-learning algorithm whereby the non-linear solver for $\rho_{X'}(\varphi, z)$ is informed by the solutions at two previous steps which allows one to exclude divergences and obtain stable solutions.

For the capacitive regime of the EDL when no (Faradaic) current except the transient one (caused by the varying electrode potential) is assumed, the boundary conditions of the MPBE for the electrostatic potential φ and the surface charge density σ are uniquely related due to the fundamental theorems of electrostatics. For these conditions, the transient current density j is directly related to the differential capacitance C_{dif} as $j = \frac{d\sigma}{dt} = \frac{d\varphi}{dt}C_{dif}$, where $\frac{d\varphi}{dt}$ is the voltage scanning rate. Both the capacitive current density and the differential capacitance are experimentally measurable quantities. On the other hand, our continuum model has direct access to $C_{dif} = \frac{d\sigma}{d\varphi}$ since both $\varphi = \varphi(\sigma)$ or $\sigma = \sigma(\varphi)$ can be computed. In either case, the electrode potential φ is referenced with respect to the its value in the bulk $\varphi|_{z\to\infty}$ which is set to zero. For a generic case when specific adsorption potentials $\Phi_X(z)$ are considered, C_{dif} accounts for the capacitance of the electrolyte near the ideally polarizable electrode whose quantum capacitance is ignored due to its negligible contribution to the overall EDL capacitance. As we shall show below, both the Helmholtz and the diffusive capacitances are included in C_{dif} calculated from our model and no further partitioning is required.

B. Specific adsorption and dielectric screening

The additional interfacial potential profiles $\Phi_X(z)$ in Eq. (5) can be generally defined, describing specific adsorption in the case of electrified interfaces or possibly free energy penalties for desolvation or transfer of ions from one dielectric medium to another. The benefit of working with the MPBE is the ease of applying different boundary conditions. Depending on the situation, this model with $\frac{d\varphi}{dz}\big|_{z\to 0} = -\frac{\sigma}{\varepsilon_0\varepsilon}$ or $\varphi(0) = \varphi_0$ describes electrode/electrolyte interfaces, whereas $\frac{d\varphi}{dz}\big|_{z\to\pm\infty} = 0$ is suitable for gas or liquid/liquid interfaces. Within the electrochemical context, for many useful/common cases, the population of ions at the interface is dominated by the effects of specific adsorption. Therefore, potentials $\Phi_X(z)$ are of key importance.

The interfacial potential profiles can be obtained from, for example, AIMD free-energy sampling for isolated ions. These potentials can be further used to obtain many-particle density profiles within the mean-field approximation. Thus, the consideration of $\Phi_X(z)$ allows us to quantitatively substitute for such *ad hoc* parameters as the thickness of the Helmholtz compact layer and its capacitance $C_c = \frac{\varepsilon\varepsilon_0}{l}$, which is important for interpretation of the shape of differential capacitance curves. By reference to Eq. (5), the adsorption potentials are defined in addition to the standard Coulombic image-charge interactions with the electrode. Therefore, for MD-sampled profiles, it will be necessary to remove such image charge electrostatic components. This can be accomplished using the Green's function consistent with the dielectric function of the electrolyte, according to $\nabla\cdot\varepsilon(\vec{r})\nabla G(\vec{r},\vec{r}') = -4\pi\delta(\vec{r}-\vec{r}')$. For slowly varying $\varepsilon(\vec{r})$, this has the following analytic solution: $G(z,z';k_\rho) = \frac{1}{k_\rho^2\varepsilon(z')}\left(e^{-k_\rho z}-1\right)$, where $k_\rho^2 = k_x^2 + k_y^2$ is the radial reciprocal momentum in cylindrical coordinates obtained from the Fourier transform in the x-y plane.

The function $\varepsilon(\vec{r})$ defines the ability of the solvent to screen the external electric field. Its spatial dependence is implicitly included in the explicit dependence on the electric field $\varepsilon(\vec{E})$[81] or the electronic charge density of solutes or electrodes[78,83] used in modern non-linear polarization models.[79] Moreover, the discontinuities of $\varepsilon(\vec{r})$ define the image charge forces. Ideally, $\varepsilon(E)$ should be obtained from the spatially resolved AIMD sampling of the dipole-dipole autocorrelation function at various surface charge densities. However, these would be very expensive calculations. Moreover, it will be affected by the presence of ions. Here, as suggested before,[82] we use a smooth "step-like" function $\varepsilon(z) = 1+\frac{\varepsilon-1}{1+\exp(-\alpha(z-z_0'))}$ that can accurately reproduce a response consistent with Booth's ansatz for $\varepsilon(E)$. However, the location of this step can be deduced from sampling of the electron density and/or nuclear density of electrolyte species in the vicinity of the electrode surface.

Equilibrium chemical potentials for ions in a binary 1:1 electrolyte are defined as follows:

$$\begin{cases} \frac{\mu_+}{k_BT} = \frac{b^3-a^3}{a^3+b^3} + \ln n_b a^3 - \frac{2a^3}{a^3+b^3}\ln(1-n_b a^3 - n_b b^3) \\ \frac{\mu_-}{k_BT} = -\frac{b^3-a^3}{a^3+b^3} + \ln n_b b^3 - \frac{2b^3}{a^3+b^3}\ln(1-n_b a^3 - n_b b^3). \end{cases}$$

This allows us to define the excess free energy of the interface caused by the external applied and adsorption potentials

$$\Delta\Omega = \Omega[\varphi,\rho_\pm] - \Omega^*[0,n_b], \tag{8}$$

where $\Omega^*[0,n_b] = \frac{2k_BT}{a^3+b^3}\int_0^\infty dz\,\ln(1-n_b a^3 - n_b b^3)$ is the free energy of the reference state of the homogeneous bulk electrolyte that at $a, b \to 0$ reduces to that of the Gouy-Chapman model $\Omega^*_{GC}[0,n_b] = -2k_BT\int_0^\infty n_b\,dz$.

C. The presence of neutral species

In the original GCEV model, the solvent is introduced in two ways. It provides the dielectric medium characterized by ε and adds an entropic steric correction to the free energy in terms of excluded volume, since in the lattice gas model each site can be occupied at most by one species (ion or solvent molecule). However, other characteristics, such as the

chemical potential or the adsorption potentials, cannot be attributed to the solvent molecules. This can be circumvented by introducing a third neutral species.[73]

In Eq. (5), we then have a term in the enthalpy, $\Phi_o(z)\rho_o$, and a mass conservation term, $-\mu_o\rho_o$, where the subscript o underscores the neutrality of the species. Due to the finite size, a_o, of the neutral species, in the entropy, we have an additional ideal gas term and a volume exclusion term. Equation (6) for the MPBE stays the same, but now $\rho_{X'}(z)$ of the charged species and $\varphi(z)$ will be renormalized by a self-consistent profile of $\rho_o(z)$. The advantage of having explicitly neutral species included is that we can use it to imitate the well-known layering of the solvent near the electrode induced by broken translational symmetry. By forcing this layering through the "adsorption" potential $\Phi_o(z)$, one can expect a transfer via volume exclusion or displacement to a modulation of ion densities $\rho_{X'}(z)$. Though palliative, this approach enables a more faithful representation of the molecular structures which can be used as an input for AIMD simulations consistent with the boundary conditions and thermodynamic equilibrium established within the continuum model.

D. Local chemical equilibria and quasi-Faradaic processes

So far we assumed, as in the absolute majority of studies using CMs, that upon equilibration of electrostatic and entropic forces, the chemical identity of species remains fixed irrespective of spatial inhomogeneity. Moreover, no other factors than those that are described earlier can contribute to the renormalization of ion densities. However, as it is well known or expected, many ions upon electrostatic or specific adsorption undergo changes of their state of charge measured by their elecrosorption valency.[94–96] The discharging of ions upon adsorption leads to collective phenomena seen in the adsorption isotherm as an effective attraction force even between like-charged ions. Even though CMs are not limited to consider only integer charges, the proper accounting for the spatially dependent charge of ions and the charge/mass balance requires more advanced models. On the other hand, the spatial profiles of ions can be dictated by chemical transformations (re-equilibration, interconversion, disproportionation, etc.), dependent on the local ion concentration. Here, we develop a self-consistent procedure for free energy minimization when chemical equilibration plays a role as important as the electrostatics.

Consider a diprotic acid at equilibrium defined by constants $\mathcal{K}_1$ and $\mathcal{K}_2$

$$\begin{aligned} H_2B &\xrightarrow{K1} HB^- + H^+, \\ HB^- &\xrightarrow{K2} B^{2-} + H^+. \end{aligned} \tag{9}$$

If $\mathcal{K}_1 \gg \mathcal{K}_2$ and $\mathcal{K}_1 \gg 1$, then in the bulk, the dominant species will be HB^- and H^+. However, in regions where there is a local deficiency of protons, the equilibrium might be shifted to B^{2-}. Therefore, at the interface, the local population of species HB^-, H^+, and B^{2-} will be different from that given by equilibration of only electrostatic and entropic forces.

The incorporation of local chemical equilibration within the GCEV model goes as follows. To begin, we take the bulk electrolyte concentrations [i.e., the limits $\rho_X(z \to \infty)$ for each species X] defined by $\mathcal{K}_1$ and $\mathcal{K}_2$ and, for a given electrode potential, we solve the MPBE to define the concentration profiles of HB^-, H^+, and B^{2-} (the concentration profile of H_2B is neglected since $\mathcal{K}_1 \gg 1$). Next, we equilibrate the profiles of HB^- and B^{2-} locally (i.e., for each z) based on constants $\mathcal{K}_1$ and $\mathcal{K}_2$ while keeping the profile of H^+ fixed. We then alternate, fixing the spatial profiles of HB^- and B^{2-} obtained at the previous step and relaxing the profile of H^+ by solving the newly constrained MPBE. These alternating steps are repeated until convergence of the concentration profiles of all species is reached. The outcomes of this iterative procedure are ion density profiles that are consistent with both local chemical equilibrium and the electrostatic potential in a manner that delivers the minimum of the free energy. The self-consistent scheme is illustrated in Fig. 1.

For the case of ions of the same size a, the MPBE for the distribution of protons, subject to the local equilibration constraints defined in Eq. (9), is written as

$$\nabla \cdot \varepsilon(z)\nabla\varphi = 4\pi e\left(2\rho^*_{B^{2-}}(z) + \rho^*_{BH^-}(z) - \frac{n_b(2+\kappa)e^{-\frac{e\varphi+\Phi_1}{k_BT}}\left(1 - a^3\rho^*_{BH^-}(z) - a^3\rho^*_{B^{2-}}(z)\right)}{1 - n_b a^3(3+2\kappa) + n_b a^3(2+\kappa)e^{-\frac{e\varphi+\Phi_1}{k_BT}}}\right), \tag{10}$$

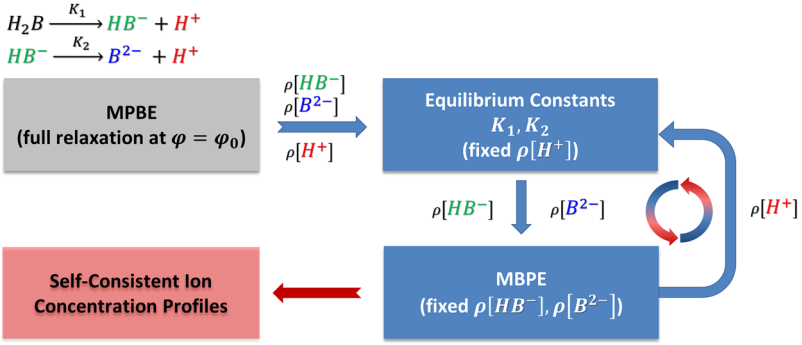

FIG. 1. Self-consistent computational scheme of evaluation of density profiles of three ions when chemical equilibration is accounted for on top of the relaxation of electrostatic and entropic forces. MPBE stands for the modified Poisson-Boltzmann equation. Conditions of each step of calculation are indicated inside each block. Captions for each arrow indicate the output of calculations at the previous step.

where $\kappa = \frac{n_b[BH^-]}{n_b[B^{2-}]}$ and $\rho^*_{BH^-}(z)$ and $\rho^*_{B^{2-}}$ are the fixed concentration profiles of the corresponding ions. For ions of disparate sizes, expressions for $\rho_{B^{2-}}(z)$, $\rho_{BH^-}(z)$, and $\rho_{H^+}(\varphi, z)$ can be obtained numerically. The described computational scheme corresponds to the physical situation when the time scale of the chemical equilibration is much faster than that of the ion migration/diffusion caused by the external field implying the high concentration limit. If the capacitive regime of the EDL is probed with sweep voltammetry, at every electrode potential, the structure of the EDL obtained from this model is valid when the normalized scan rate is much slower than the equilibrium reaction rates $\mathcal{V} = \frac{e}{k_B T}\frac{d\varphi}{dt} \ll \mathcal{K}$. It is worth mentioning that we assume no spatial dependence in the equilibrium constants, which could easily be modified very close to the interface merely due to the broken translational symmetry or steric constraints. However, if needed, this information might possibly be accessible through exploring the free-energy profiles for specific chemical conversions using AIMD.

Finally, there are experimental situations when the equilibrium is being reached in conditions when at least one of the species is controlled by the chemical potential not in the bulk but at the electrode. This is the typical situation for electrochemical metal dissolution when, upon changing the electrode potential, new cationic species emerge at the interface. Here we show how the GCEV model can be modified to include this functionality. We start with a three ion free energy functional

$$\begin{aligned}\Omega[\varphi;\rho_\pm,\rho'] = \int dz \Bigg(&-\frac{\varepsilon(z)}{8\pi}|\nabla\varphi|^2 + e\varphi(\rho_+ - \rho_- + \zeta\rho') \\ &+ \Phi_+\rho_+ + \Phi_-\rho_- + \Phi'\rho' - \mu_+\rho_+ - \mu_-\rho_- - \mu'(\varphi)\rho' \Bigg) \\ &+ \frac{k_B T}{a^3}\int dz\, a^3\rho_+ \ln a^3\rho_+ + \frac{k_B T}{b^3}\int dz\, b^3\rho_- \ln b^3\rho_- \\ &+ \frac{k_B T}{c^3}\int dz\, c^3\rho' \ln c^3\rho' + \frac{3k_B T}{a^3+b^3+c^3} \\ &\times \int dz\,(1 - a^3\rho_+ - b^3\rho_- - c^3\rho') \\ &\times \ln(1 - a^3\rho_+ - b^3\rho_- - c^3\rho'), \end{aligned} \tag{11}$$

where ρ' is the density profile for the cationic species produced at the electrode, ζ is its charge, and $\mu' = \mu'(\varphi)$ is its chemical potential, which, for the sake of simplicity, we consider as a function of the electrode potential only. In more realistic situations, μ' should depend on the chemical potentials of other species as well, as in the case of metal dissolution assisted by specifically adsorbing anions. In contrast to $\mu_\pm$, defined to guarantee the bulk concentration n_b, the requirement for $\mu'(\varphi)$ is to be sufficiently negative at potentials $\varphi < \varphi_c$ to have the population of $\rho'(z) \sim 0$ at large distances where all potentials are zero. An additional constraint could be placed on $\mu'(\varphi)$ to guarantee a certain amount of new species at the interface for a given electrode potential $\int_0^\infty dz\,\rho'(z)|_{\mu'=\mu'(\varphi)} = f(\varphi)$. Since we do not consider entropic forces associated with diffusion, nor any time-dependence (see Sec. III), the proposed model describes an instantaneous equilibrated distribution of all species as a result of a quasi-Faradaic process in the limit of infinitely slow diffusion rate. Despite its *ad hoc* character, this model enables rough estimates of emerging species as a function of their charge ζ, which can help clarify details of interfacial speciation and the interpretation of surface sensitive spectroscopy measurements. Moreover, different ingredients of the proposed model can be combined to simulate various conditions that may be relevant to a given experiment.

III. RESULTS AND DISCUSSION

A. Building complexity into the GCEV description of a mixed electrolyte

We start by considering the aqueous solution of three ions (K^+, F^-, and Br^-) and minimizing the GCEV free-energy functional [Eq. (6)], obtaining $\rho_{K^+}(\varphi)$, $\rho_{F^-}(\varphi)$, and $\rho_{Br^-}(\varphi)$ from a numerical solution of equations $\frac{\delta\Omega}{\delta\rho_i} = 0$. First, we consider the case when all the adsorption potentials are zero, $\Phi_X(z) = 0$. The spatially dependent dielectric is modeled by a smoothened step-like function $\varepsilon(z) = 1 + \frac{\varepsilon - 1}{1 + exp(-\alpha(z - z'_0))}$, where $\alpha = 5$ Å^{-1} and $z'_0 = 0.5$ Å and we use the bulk dielectric constant of water, $\varepsilon = 80$.

1. Ion-size disparity

In Fig. 2, we show the results of calculations for three cases corresponding to three combinations of effective ion diameters. The bulk concentrations of all ions were fixed for all three cases, $n_b(K^+) = 1$M, $n_b(F^-) = 0.5$M, and $n_b(Br^-) = 0.5$M. In Fig. 2(a), we show the fully symmetric case when all ions are of the same size. The upper panel shows the polarization curves, an alternate representation of the density profiles, illustrating their dependence on the computed potential $\rho_{ion}(\varphi)$, independent of the spatial coordinate z. At potential $\varphi = 0$, $\rho_{K^+} = 1$M and $\rho_{F^-/Br^-} = 0.5$M, which corresponds to the concentrations in the bulk electrolyte. In this particular panel, the anions are indistinguishable (*viz.*, the same charge and the same effective radius) and the polarization curves for F^- and Br^- coincide, with their common upper bound being ≈6.6M, as defined by the lattice saturation within the GCEV model at high positive potentials. For cations, this upper bound is ≈13.28M. These values correspond to the maximum interfacial concentrations of ions at sufficiently high potentials. Accordingly, the differential capacitance curve (lower panel) is fully symmetric, with the potential of zero charge (PZC) appearing at $\varphi = 0$. In Figs. 2(b) and 2(c), we illustrate the effect of ion-size disparities. The polarization curves show that at high enough positive potentials, a smaller anion (F^- in this case) will be dominant, suppressing the larger anion (Br^-) concentration. The differential capacitance maximum at $\varphi \approx 0.1$ V [Fig. 2(b)] is only slightly reduced, since we consider the case of three ions with one of the anions equal in size to the cation ($a_{K^+} = a_{F^-} = 5$ Å). There is a more noticeable effect of size disparity in the two-ion case, for example, with effective sizes of cations and anions

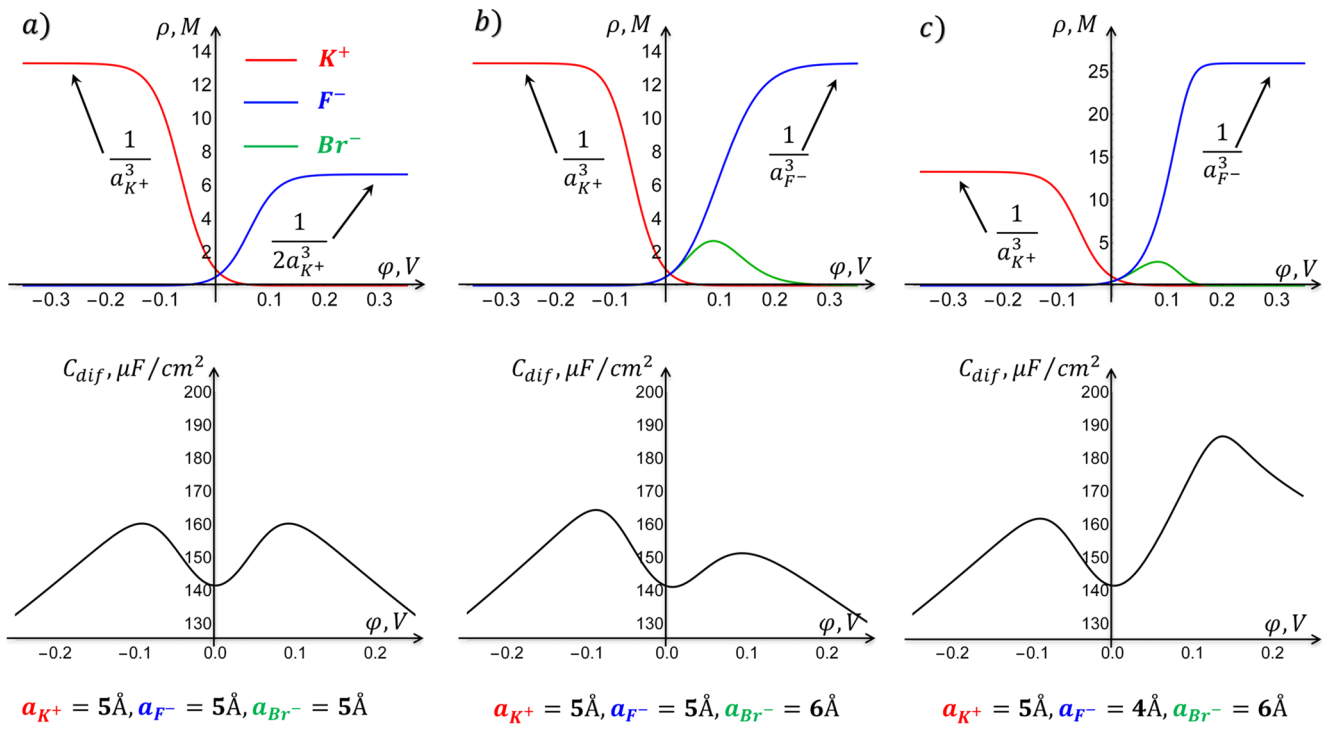

FIG. 2. Polarization curves $\rho(\varphi)$ (upper panels) and differential capacitances $C_{dif}(\varphi)$ (lower panels) for a three-ion solution of K^+, F^-, and Br^- with various combinations of ion sizes. The bulk concentrations are $n_b(K^+)$ = 1M, $n_b(F^-)$ = 0.5M, and $n_b(Br^-)$ = 0.5M. The lattice saturation concentrations are indicated by arrows.

of 5 and 6 Å, respectively. We illustrate this effect in the three-ion system in Fig. 2(c), where one of the anions is smaller than the cation and the increase of C_{dif} is much more prominent. This is consistent with the possibility that spatial regions with positive potentials will be populated more densely by smaller anions, thereby increasing the charge density response.

2. Non-zero adsorption potentials

Next, we consider the case for non-zero adsorption potentials, $\Phi_X(z) \neq 0$. We explore the situation when one of the anions (Br^-) is specifically adsorbing whereas the potentials of the other two species (K^+ and F^-) are repulsive, preventing those ions from direct contact with the electrode, for example, due to strong solvation. The adsorption potential for Br^- has a Morse form defined by $\Phi_{Br^-} = E_{ads}(1 - e^{-\kappa(z-z_0)})^2 - E_{ads}$, where E_{ads} = 0.15 eV, $\kappa = 1$ Å^{-1} and z_0 = 2.4 Å. The potentials Φ_{K^+} and Φ_{F^-} are smoothened hard walls with a small mismatch at around 3 Å [see Fig. 3(a)]. Now, since the free energy functional has attained a non-electrostatic part, the solutions to the minimization, ρ_{ion}, will each have an explicit z-dependence: $\rho = \rho(\varphi, z)$. Consequently, the polarization curves at a specific potential can vary at different distances from the electrode, as shown in Figs. 3(b)–3(d). Importantly, at some distances, the larger specifically adsorbing ions (Br^-) dominate the entire

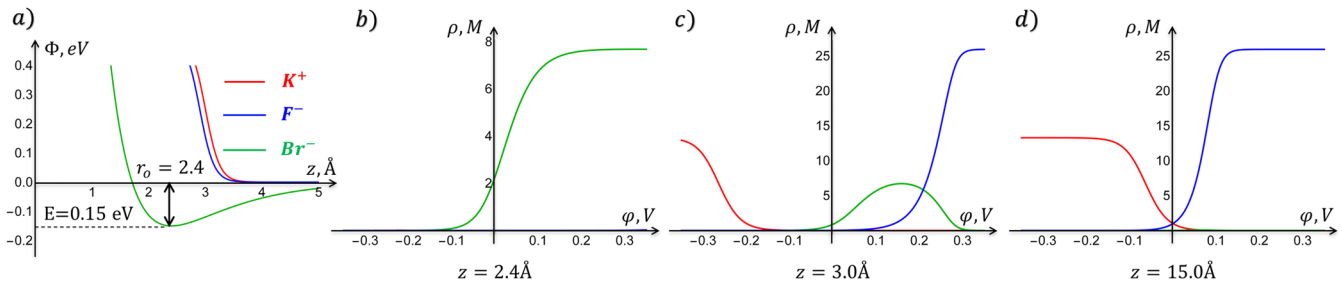

FIG. 3. Adsorption potentials (a) and polarization curves $\rho(\varphi, z)$ for a three-ion solution K^+, F^-, and Br^- [(b)–(d)]. The distances are indicated below each graph. The sizes of ions are 5, 4, and 6 Å for K^+, F^-, and Br^-, respectively. The bulk concentrations are $n_b(K^+)$ = 1M, $n_b(F^-)$ = 0.99M, and $n_b(Br^-)$ = 0.01M.

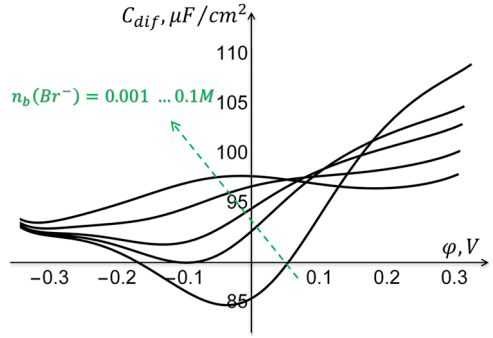

FIG. 4. Progression of differential capacitance with specific adsorption of Br^- anions. Adsorption energies E_{ads} = 0.15 eV for concentrations $n_b(Br^-)$ = 0.001, 0.01, 0.02, 0.05, 0.1M.

potential range, whereas at other distances there is a competition between F^- and Br^-. Far from the electrode where $\Phi_{Br^-} = 0$ [Fig. 3(d)], we see smaller anions dominating at any positive potentials.

Clearly, the presence of non-zero adsorption potentials has a profound effect on the differential capacitance. Even a small concentration of specifically adsorbing ions can drastically modify the profile. In Fig. 4, we show a progression of the differential capacitance with the concentration of Br^--ions while keeping the same ionic strength of the solution $n_b(K^+)$ = 1M. At the smallest concentration, $n_b(Br^-)$ = 1 mM, there is a slight shift of the PZC to negative values, as expected for specifically adsorbing anions. The differential capacitance curve is much broader and its values at positive potentials are higher due (as before) to the smaller size of F^--ions as compared to that of cations. At $n_b(Br^-)$ = 0.01M, the differential capacitance loses its symmetry [compare to Fig. 3(c) with the minimum moved to the negative potential $\varphi \approx -0.1$ V]. It still resembles the "camel"-like shape with maxima lying beyond the ±0.3 V range. As the concentration of specifically adsorbing ions increases, C_{dif} evolves into the curve with multiple minima, without any resemblance to canonical differential capacitance curves with well-defined minima at the PZC. At sufficiently negative potentials to desorb any specifically adsorbed anions, the effect of the specific adsorption potential vanishes and all curves coincide. It should be noted that similar trends were experimentally observed for simple anions at polycrystalline silver-aqueous interfaces.[97] Higher adsorption energies would modify the profiles even at smaller concentrations, producing "bell"-like curves. This example shows that a combination of simple factors may result in a complicated overall effect and highlights the importance of realistic electrolyte models for the interpretation of measured differential capacitance of non-ideal electrolytes.

3. Implications for air/liquid interfaces

Another important feature of our GCEV model is that it enables description of other types of interfaces, e.g., air/liquid interfaces. We can achieve this by adjusting the boundary conditions such that the gradient of the potential far from the interface vanishes, $\frac{\partial \varphi}{\partial z}\Big|_{z\to\pm\infty} = 0$, and then solving the MPBE over the entire range of z in $[-\infty.\infty]$. The control parameter is now not the electrode potential—we have no electrode—but rather the adsorption potentials for ions. $\Phi_X(z)$ describes the single particle free energy of ions, including the desolvation energy, as ions emerge from the liquid into air/vacuum. In this case, the self-consistent electrostatic potential φ describes the contribution from the ions and ignores the surface potential drop originating from the surface excess dipole of the pure solvent. The latter affects the ion spatial distribution and, in turn, becomes affected by the ionic component. The self-consistent description of the overall effects within the phenomenological free energy functional (MPBE) would require far more advanced modeling and can be rigorously considered in the framework of the CDFT.[53,69,70] The importance of the dipolar contribution still depends on the electrolyte composition and concentration. However, single particle free energy adsorption potentials $\Phi_X(z)$ obtained empirically from AIMD calculations will include dipolar effects. Thus our model can still, at least partly, implement the missing phenomenology.

However, in this approximation, our GCEV model still includes the image charge effects and provides an estimate of the potential drop across the interface. In Fig. 5, we show the ion density profiles and corresponding profiles of the self-consistent electrostatic potential for a model binary 1:1

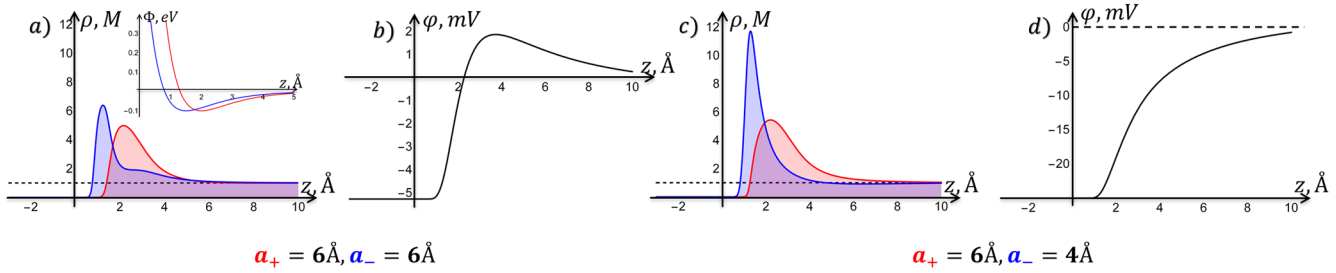

FIG. 5. Ion density profiles [(a) and (c)] and the profiles of the self-consistent electrostatic potential [(b) and (d)] at the air/liquid interface for a binary 1M 1:1 solution of ions (with, without) size disparity. The parameters of the dielectric function are described in the text and the ion adsorption potentials are shown in the inset.

solution characterized by a slight mismatch of the effective adsorption potentials $\Phi_X(z)$ for anions and cations and consider the effect of the ion-size disparity. As illustrated, both the potential drop and the potential profile are sensitive functions of ion-size disparity.

By definition, the calculated potential drop is the Galvani potential that determines the work required to bring a probe (non-perturbing) unit charge particle from infinity to the bulk liquid. The positive drop of the potential (left-to-right) in the electrostatic convention means that the regions with negative potential are attractive for negatively charged species. Therefore, the extra anionic species, if present in the bulk, will be attracted to the interface (as long as their population does not change the overall electrostatic profile) from the bulk liquid. As illustrated, both the potential drop and the potential profile are sensitive functions of ion-size disparity. For the interface populated with equally sized ions, extra anions will have to overcome the potential barrier to come from the bulk liquid, as shown in Figs. 5(a) and 5(b). By contrast, if the size of anions is smaller than that of cations, extra anionic species experience no barrier to populate the interface, as shown in Figs. 5(c) and 5(d). Thus, the proposed functionality of our GCEV model could be useful to justify certain assumptions about the anatomy of the liquid interfacial layers and microscopic factors that result in it. Specifically, this approach could be applied to study the Jones-Ray effect and analyze the role of surfactant impurities.[98–100]

4. Theoretical adsorption isotherms

Returning to the electrode/electrolyte interface, further insight into the structure of the EDL can be obtained from an analysis of the surface excess of adsorbed species and associated adsorption isotherms, which link the thermodynamics of the interface with its structure or composition. From an experimental measurement standpoint, following early ideas of Grahame[13] and, subsequently, Parsons's analysis of the relationship between the EDL capacitance and the surface excess of adsorbed species,[14] one can estimate the number of adsorbed molecules (per unit area) using the "Hurwitz-Parsons" analysis of differential capacitances.[16] This can be further converted into adsorption isotherms.[101,102] Altogether, such analysis of experimental capacitance data reveals thermodynamic details embedded within the ion adsorption potentials, such as lateral ion interactions in the adsorbed states and their dependence on surface charge or electrode potential.

From our theoretical perspective, the continuum theory described above, that includes the effects of specific adsorption, provides direct access to the surface coverage and so to the adsorption isotherm and its parameters. The comparison between such experimental and theoretical analyses provides the means for validated refinement of the parameters of the continuum model. Furthermore, it provides a thermodynamic picture of the interfacial electrolyte structure (e.g., the EDL) at various potentials which is extremely useful for interfacial AIMD simulations: providing initial conditions and guaranteeing thermodynamic stability of the interfacial molecular structure.

Here, we analyze the surface excess of specifically adsorbed Br^--ions that we obtain from our GCEV model and derive the parameters of the adsorption isotherms. The coverage θ is obtained as $\theta_X = \frac{1}{\Gamma_S}\int_0^{z_X} dz\rho_X(z)$, where Γ_S is the maximum coverage (geometrical estimates), $z_X = z_{0X} + a_X - \frac{\ln 2}{\kappa_X}$ and $z_{0X} - \frac{\ln 2}{\kappa_X}$ is the zero of the Morse adsorption potential $\Phi_X(z) = E_{ads}(1 - e^{-\kappa_X(z-z_{0X})})^2 - E_{ads}$ and a_X is the size of the species. For simplicity, the dielectric function was set constant $\varepsilon(z) = \varepsilon$.

In Fig. 6(a), we show the percentage surface coverage, θ, as a function of electrode surface charge density, σ, at various bulk concentrations of Br^- ions in an electrolyte also containing K^+ and F^- ions, with a fixed ionic strength of 1M. The depth of the adsorption potential for the Br^--ions is set to be 0.15 eV [see Fig. 3(a)]. The maximum coverage of 1.36×10^{-9} mol cm^{-2} (one ion per 12.2 Å^2) is estimated based merely on geometrical considerations, assuming the Br^- ionic radius to be 1.97 Å.[97] The effective sizes of K^+ and F^- are set to be 4 Å. This approach ignores the structure of the electrode–the density or spatial arrangement of adsorption sites for

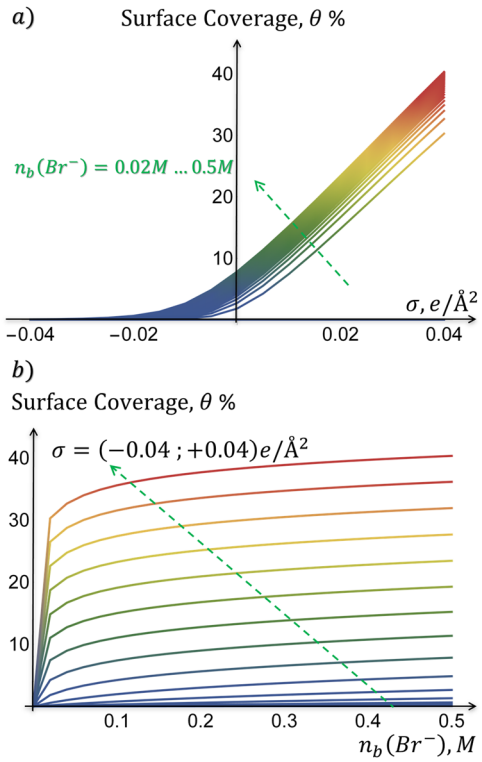

FIG. 6. (a) Surface coverage of Br^--ions in the KF/KBr electrolyte of a fixed ionic strength of 1M as a function of surface charge density at various bulk concentrations of Br^--ions. (b) Adsorption isotherms at various surface charge densities.

Br^-–thus overestimating the coverage. For a negatively charged surface, one may expect a finite coverage of Br^--ions. For a neutral surface, this plot suggests that the coverage may not exceed 10%. This is equivalent to coverage of one ion per 122 $Å^2$ in this range of concentrations.

In Fig. 6(b), the theoretical adsorption isotherms are shown at various electrode charge densities. These isotherms illustrate the dramatic effect of the specific adsorption potential, causing the surface coverage to abruptly reach its saturated magnitude (at a given surface charge density) at small bulk concentrations such that its further increase affects only slightly the surface coverage.

Another way of looking at these isotherms is by comparison with the phenomenological Frumkin isotherm

$$Bn_b = \frac{\theta}{1-\theta} e^{g\theta}, \tag{12}$$

where θ is the coverage, $k_B T \ln B = -\Delta G$ is the standard free energy of adsorption of species at a given charge on the electrode, and $g = g(\sigma)$ is the non-ideality coefficient that describes mutual repulsion between adsorbates at high coverage, which is zero for the Langmuir isotherm. Originally proposed to describe the effects of specifically adsorbing organic solvent molecules, here we use the Frumkin isotherm to explore the thermodynamics of specifically adsorbing bromide ions whose interfacial density profiles are obtained from our continuum model. By plotting $\ln n_b - \ln \frac{\theta}{1-\theta}$ as a function of θ for each bulk bromide concentration and varying the charge on the electrode, we can extract the adsorption free energy $\Delta G(\sigma)$, from the intercept at zero coverage, and $g(\sigma)$, from the slope. In this way, we can explore how microscopic single particle parameters (ion size and specific adsorption potentials) affect the macroscopic ensemble characteristics.

In Fig. 7(a), we show the progression of $\Delta G(\sigma)$ for various depths of adsorption potentials of single bromide ions $\Phi_{Br^-}(z)$. By definition, the adsorption isotherm defines the interfacial coverage that is in equilibrium with the bulk electrolyte of a given concentration. ΔG then contains all the factors that contribute to the adsorption, including electrostatic and non-electrostatic forces averaged over the grand-canonical ensemble. Surprisingly, for the range of single particle specific adsorption potentials [see Fig. 3(a)], Φ = 0.05–0.25 eV, the adsorption free energies on the neutral surface are in the range of 80–100 kJ/mol, which is very close to the reported experimental values for Br^--ions on single crystal surfaces of gold and silver.[97,103] Clearly, this matching with experimental values is rather coincidental since many other factors may have canceled each other. The partial discharging of Br^--ions upon adsorption may affect both the image charge interaction and the ion desolvation energy resulting in net specific adsorption potentials Φ_{Br^-} much smaller than the associated thermodynamic free energies $\Delta G(\sigma)$. However, this promising matching may indicate some theoretical "shortcuts" that could greatly simplify the description of specific adsorption.

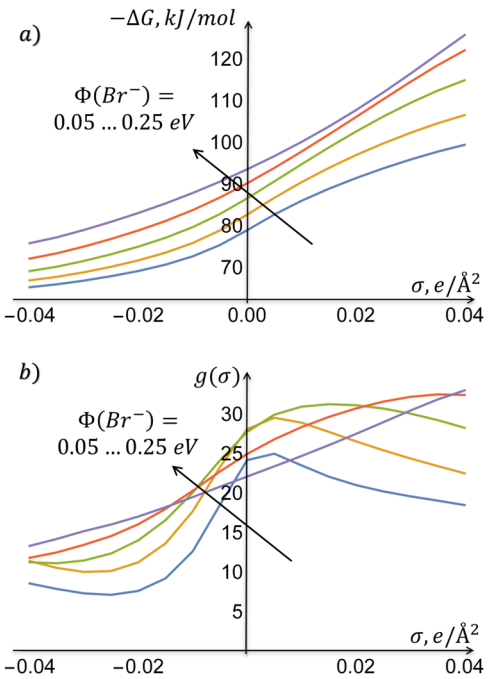

FIG. 7. (a) Adsorption free energies ΔG of Br^--ions as a function of the surface charge density extracted from Frumkin's isotherms [Eq. (12)] obtained for the KF/KBr electrolyte of a fixed ionic strength of 1M. (b) Non-ideality coefficient g as a function of the surface charge density. Both $\Delta G(\sigma)$ and $g(\sigma)$ are parameterized by the single particle adsorption potential depths Φ [see Eqs. (5) and (11)]. Color schemes for (a) and (b) are the same.

Another important finding is that the adsorption free energy is a non-linear, though monotonic, function of the surface charge density or electrode potential: $\Delta G(\varphi) \neq \Delta G_o + e\varphi$. Figure 7(b) shows a peculiar dependence of the extracted coefficient g [Eq. (12)] in the Frumkin isotherm that characterizes the interactions between adsorbed ions. Its positive values imply effective repulsion. In our GCEV model, the adsorbed ions retain their bulk oxidation state charges (there is no charge transfer included). Therefore, the decrease of g at higher surface charge density, σ, signifies the effect of crowding of Br^--ions at positively charged surfaces such that the minimization of the free energy with the term $g\theta^2$ appears as effective lowering of anion-anion repulsion. Entropic and enthalpic factors may even result in an effective attraction between like ions, making g negative, which would lead to hysteresis in adsorption/desorption regions of the electrode potential and peculiar "phase-transitions" in the adsorbed layers triggered by a small change in the charge on the electrode.

This analysis shows that our continuum model provides tantalizing links between the atomistic picture, with single particle descriptors, and the equilibrium thermodynamics of the interface. Moreover, we can relate the details of a single particle adsorption potential $\Phi(z)$ with a mean-field description of the adsorption isotherm. Indeed, as Parsons showed,[14]

the difference between the inverse capacitances of a reference electrolyte and an electrolyte containing specifically adsorbing ions has the following relation:

$$\frac{1}{C_o} - \frac{1}{C} = k_B T\left(\frac{\partial^2 \ln B}{\partial \sigma^2}\Gamma_{Br^-} + \left(\frac{\partial \ln B}{\partial \sigma}\right)^2 \frac{\partial \Gamma_{Br^-}}{\partial \ln B}\right), \quad (13)$$

where Γ_{Br^-} is the surface excess of Br^- ions and $k_B T \ln B = \Delta G$. Originally, this equation was used to define the applicability of different forms of the adsorption isotherm. Here, we can show that this equation permits testing the dependence of ΔG on the charge density and thus on the adsorption profile, $\Phi(z)$. Assuming a linear dependence of $\Delta G(\sigma)$ in the dilute regime, when the adsorbed layer obeys Henry's law, $\Gamma_{Br^-} = B\, n_b$, Eq. (13) reduces to[15]

$$\frac{1}{C_o} - \frac{1}{C} = k_B T\left(\frac{\partial \ln B}{\partial \sigma}\right)^2 B n_b, \quad (14)$$

implying that $\Delta\left(\frac{1}{C}\right)$ is positive. As can be shown, adsorption profiles, $\Phi(z)$, that do not have a repulsive wall lead to negative $\Delta\left(\frac{1}{C}\right)$. Generally, Eq. (13) can be seen as the differential equation for the unknown function $\Delta G(\sigma)$ when C_o and C are known functions of surface charge density.

5. Free energy analysis

Evaluation of free energies associated with particular profiles of ions near the interface is important for two main reasons. First, $\Delta\Omega$ [see Eq. (8)] enables evaluation of the relative probability of different ion profiles. This can be directly related to estimates of the probability distribution of fluctuations within the ion density profiles. This is vital for assessing the thermodynamic stability of the interface. Second, the free energy (per unit area) is directly related to the surface tension. Therefore, its theoretical estimates permit a direct comparison with experimentally measured observables and provide insights into the structure of the EDL at various surface charge densities.

Here, we evaluate the free energy costs with respect to the homogeneous bulk electrolyte associated with charging the surface of the electrode and explore the role of specific adsorption potentials. Specifically, we consider a symmetric 1:1 binary 1M electrolyte with ions of effective sizes $a_{K^+} = 6$ Å and $a_{Br^-} = 4$ Å for cations and anions, respectively. Our functional [see Eq. (5)] does not explicitly account for the effects of the solvent (water) apart from employing a non-linear dielectric function profile $\varepsilon(z)$. Therefore, we evaluate just the ionic contribution to the electrolyte surface tension and ignore the free charge component associated with the electrode itself.

In Fig. 8, we show the surface free energies ΔG in units of N/m. The positive values mean that there is a free energy gain upon immersion of a charged electrode into an electrolyte ("ionophilic" electrode), whereas negative values imply that the immersion is energetically unfavorable ("ionophobic" electrode). When no adsorption potentials are applied [Fig. 8(a)], the negative of the free energy is slightly asymmetric (due to the differing ion sizes) with its minimum at $\varphi = 0$ meaning that the immersion is favorable at any charge (positive or negative). For water, the surface free energy against air is ~72 dyn/cm (or 0.072 N/m),[104] implying that our model predicts a comparable ionic contribution at $\varphi = 0.3$ V vs. PZC for non-adsorbing ions. A contrasting situation, when the electrode equally repels ions at neutral conditions, is shown in Fig. 8(b). Unless the electrode is sufficiently charged (around ±0.1 V), the "ionic wetting" remains unfavorable. For the case when at least one ionic species—the anions here—is specifically adsorbing [Fig. 8(c)], the free energy is always negative with the minimum shifted to negative potentials and enhanced values at positive potentials. At sufficiently negative potentials $\varphi < -0.2$ V, the free energy curves for case (b) and case (c) coincide [see the inset in Fig. 8(c)] indicating that the anions have electrochemically desorbed.

Thus, our GCEV model restores remarkably well-known electrocapillary curves.[5] The shape of the free energy curves is close to quadratic as in the original Frumkin theory.[102] It is quite surprising that the GCEV model reproduces such a

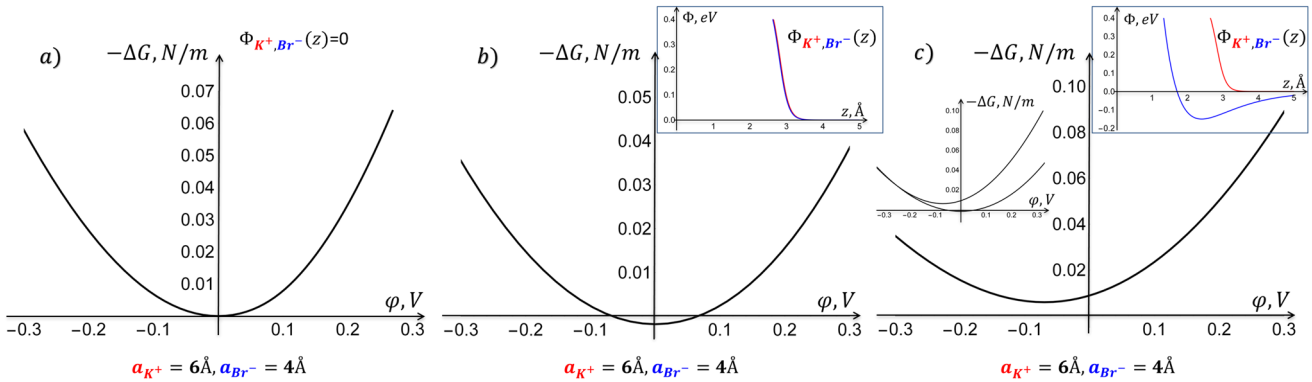

FIG. 8. Surface free energy as a function of the electrode potential for various ion adsorption potentials (see the insets): a case of a binary 1M electrolyte KBr. Sizes of ions are 6 Å and 4 Å for K^+ and Br^-, respectively. (a) Surface free energies without adsorption potentials for ions. (b) Surface free energies when adsorption potentials are purely repelling for both ions. (c) Surface free energies when anions are specifically adsorbing and cations are repelled from the electrode.

simple shape of the free energy curve as well as its other main features (e.g., the proper shift of the minimum in the presence of surface active anions) given its advanced mathematical formulation. However, in contrast to the previous phenomenological formulations, this model includes microscopic descriptors [e.g., the single particle adsorption potential $\Phi_X(z)$, ion size, etc.] which provide additional insights into the anatomy of the EDL and open up pathways to engineer the molecular or nanoscale composition at interfaces. It would be then interesting to explore the factors that could give rise to multiple minima in the surface free energy. In this regard, the proposed model, when applied to air-liquid interfaces, could be useful to elucidate the role of ions and their contribution to the Jones-Ray effect[98] in which a minimum in the surface tension is observed at mM salt concentrations.

B. Effects of local chemical equilibration

Here we consider a model case of a diprotic acid in equilibrium with an electrode to show how the interfacial structure of the EDL can be affected by local chemical equilibrium. We assume that the equilibrium in Eq. (9) is characterized by the equilibrium constants $\mathcal{K}_1 = 1000$ and $\mathcal{K}_2 = 0.01$. This is a typical case for dilute solutions of strong acids (e.g., H_2SO_4) where, despite full dissociation of the acid, the dominant species are HB^--ions (it is only weakly diprotic in water). The equilibrium concentrations in the bulk of a 0.1M solution of H_2B are 0.0915M, 0.1084M, 0.008 44M, and 9.92×10^{-6}M for HB^-, H^+, B^{2-}, and H_2B, respectively. We also assume that HB^- and B^{2-} ions are specifically adsorbing with the parameters of their adsorption potentials being $E_{ads} = 0.14$ eV and 0.12 eV, respectively. $z_0 = 2.7$ Å, and $\kappa = 4$ Å^{-1}. We assume a purely repulsive potential for H^+-ions with the wall at $z = 2.5$ Å. For simplicity, the dielectric function was set constant $\varepsilon(z) = \varepsilon$. The length scale of the ionic screening of the surface charge density is defined by the Gouy-Chapman length $l_{GC} = \frac{2\varepsilon k_B T}{e\sigma}$. For $\sigma = 4.8\,\mu C/cm^2$ and $\sigma = 9.6\,\mu C/cm^2$, the Gouy-Chapman lengths are 7.6 Å and 3.8 Å, respectively. In Fig. 9, we show ion density profiles at various surface charge densities for three different cases. In Figs. 9(a)–9(d), we show the profiles of ions of equal size (6 Å) when no local chemical equilibration is assumed. In Figs. 9(e)–9(h), we show how density profiles are modified by instantaneous chemical equilibration. The most striking output from these calculations is the significant enhancement in population of minor B^{2-} ions at the interface at positive surface charge density when an additional mechanism of equilibration is accounted for. The effect of ion size disparity is shown in Figs. 9(i)–9(l). Since the size of protons is smaller here, the enhancement of the B^{2-} is weaker due to the higher proton concentration at the EDL. At more positive surface charge densities, the population of B^{2-} is expected to be even higher due to the combination of effects of electrostatic attraction and the shift of equilibrium to B^{2-} caused by depletion of protons at the EDL. Therefore, despite the fact that the bulk concentration of B^{2-}-ions is more than an order of magnitude lower than that of HB^-, in certain surface charge regimes, the EDL may be noticeably populated with B^{2-}-ions simply due to the local chemical equilibrium. This effect should be more pronounced for solutions with a lower bulk concentration of H_2B.

We highlight some shortcomings of these calculations. The free energy minimization does not include entropic costs associated with ion diffusion such that the ion density profiles are subjected to additional modifications (smoothing). However, it remains largely unclear how to incorporate the ion diffusion coefficients into the current theoretical framework. Generally, accounting for entropy-driven ion diffusion requires minimization of the entropy production functional,[105,106] whose variation gives rise to the diffusion or heat transport equations, but not the grand canonical free energy functional.

C. Effects of neutral electrolyte species

Equation (5) can easily include additional neutral species in the electrolyte, characterized by the chemical potential μ_o, the adsorption potential $\Phi_o(z)$, and the effective size a_o. Neutral species do not contribute directly to the MPBE but affect the ion distribution via the entropic term that couples the densities of all species (via volume exclusion). In addition, if the corresponding adsorption potential is nonzero, $\Phi_o \neq 0$, the ions and neutral species will compete at the electrode surface, which will also modify the resulting ion profiles. Thus, inclusion of explicit neutral species in our GCEV model can mimic the actual solvent whose density variations modulate the ion density profiles. The adsorption potential Φ_o provides the means to imitate the densification of the solvent at the electrode surface without the necessity of introducing nonlocal functionals. The theoretical foundation for this operation is the fundamental relationship $-k_B T \frac{\delta \ln Z(\Phi)}{\delta \Phi(r)}\Big|_{\Phi \to 0} = \rho_1(r)$ between the single-particle distribution function and the functional derivative of the free energy over the external potential at the limit of $\Phi \to 0$.[107] Therefore, Φ-potentials are not just single particle free energy adsorption potentials and may also include other correlation effects missing at the LDA-MF approximation. As long as we work in the linear response regime and disregard all finer two-, three-, and higher order particle-particle correlations, this relationship enables one, at least in principle, to restore the external (effective) potential from $\rho_1(r)$ and replace a non-local Hamiltonian by an effective Hamiltonian with an external potential that gives rise to the same $\rho_1(r)$ (of, e.g., neutral species). In reality, due to the specific adsorption of the solvent on the electrode surface, the ions must compete with solvent molecules and this effect would not be possible to include in the standard GCEV model merely via only steric factors among the ions.

In Fig. 10, we compare the ion density distributions in a binary 1:1 0.5M electrolyte with and without neutral species at various surface charge densities. The ion sizes were set as 6 Å and 4 Å for cations and anions, respectively, and the size of neutral species was set as 5 Å. The bulk concentration of solvent is 10M. In Figs. 10(a), 10(c), and 10(e), we show the profiles of ions without neutral species. The adsorption potentials $\Phi_{1,2}(z)$ are shown in the inset of Fig. 10(e). Here, we consider specific adsorption of anions (blue curve) whereas cations, due

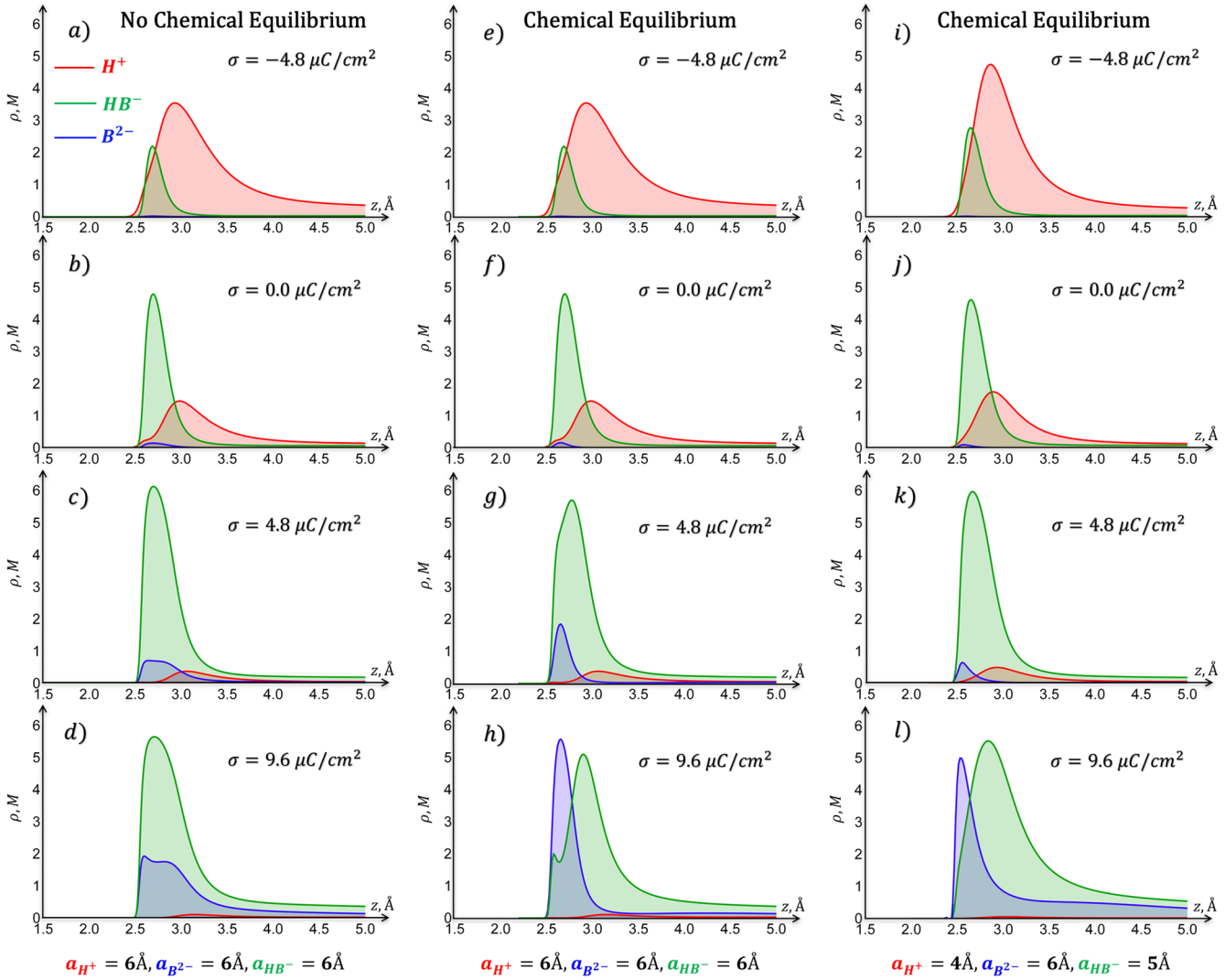

FIG. 9. Density profiles of H^+, HB^-, and B^{2-} with bulk concentrations defined by the equilibrium constants $\mathcal{K}_1 = 1000$ and $\mathcal{K}_2 = 0.01$ [see Eq. (8)] near the electrode surface at various assumptions. [(a)–(d)] Profiles of ions of size 6 Å for different charge on the electrode when no chemical equilibrium is assumed. [(e)–(h)] Profiles of ions of size 6 Å for different charge on the electrode with instantaneous chemical equilibrium. [(i)–(l)] Profiles of ions of sizes 4 Å, 6 Å, and 5 Å for different charge on the electrode with instantaneous chemical equilibrium.

to their higher solvation energies, cannot approach quite as near to the surface, which is modeled by a repulsive potential (red curve).

Due to specific adsorption, the anion density profiles demonstrate characteristic peaks [more prominent near the neutral and positively charged surfaces, Figs. 10(a)–10(d)] accompanied by waves of cation density due to Coulombic attraction. The adsorption potential of the neutral species, $\Phi_o(z)$, is shown by a green curve. It is designed to mimic the solvent layering at a hard-wall interface. The "polarization curves" in the bulk solvent are shown in the inset of Fig. 10(a).

It shows that at higher potentials, the solvent molecules are replaced by the ions whose density profiles are modified by the solvent. The inclusion of neutral species brings two new effects. First, the modulations of ion density profiles with multiple maxima are much more pronounced and steric competition makes the cation density more compact (compare red profiles in the upper and the lower panels in Fig. 10). Second, ion densities become renormalized as compared to the case without neutral species. Moreover, the profile of neutral species depends on the charge on the electrode due to the self-consistency of the solution to the MPBE. Therefore, when combined with other interfacial features, this approach

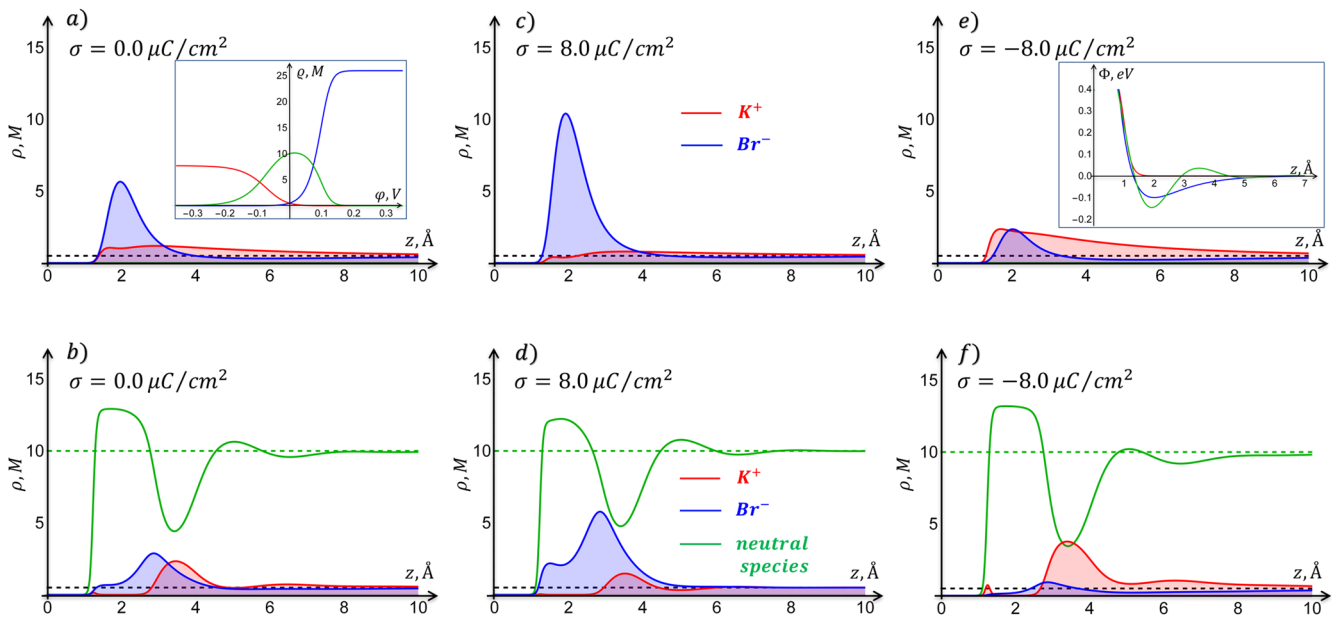

FIG. 10. Effects of the explicit presence of neutral species on the ion density profiles of the binary 0.5M electrolyte KBr at various electrode surface charge densities. Polarization curves $\rho_{K^+,Br^-,o}(\varphi)$ and the adsorption potentials $\Phi_{K^+,Br^-,o}(z)$ are shown in the insets [(a) and (e)]. Panels (a), (c), and (e) show the profiles of ions in the absence of neutral species. Panels (b), (d), and (f) show the effects of neutral species (bulk concentration is set as 10M). The sizes of species are 6 Å, 4 Å, and 5 Å for cations, anions, and neutral molecules, respectively. Red, blue, and green colors are used for cations, anions and neutral molecules, respectively.

is able to provide a variety of phenomenologies and more closely matches observed behavior from sampling of AIMD trajectories.

D. Quasi-Faradaic processes

Finally, we consider the case when the electrode acts as a reservoir, not only of electrons but also of other (ionic) species which can emerge into the electrolyte at certain potentials. Specifically, if we know the chemical potential of these species, and its electrode potential dependence, $\mu' = \mu'(\varphi)$, then we can use our GCEV model [Eq. (11)] to determine their density profile $\rho'(z)$. This is of particular interest in the case of electrochemical metal dissolution. The minimization of the GCEV functional describes the competition between "chemical" forces that produce new species at the interface and the electrostatic forces that redistribute ions according to the boundary conditions.

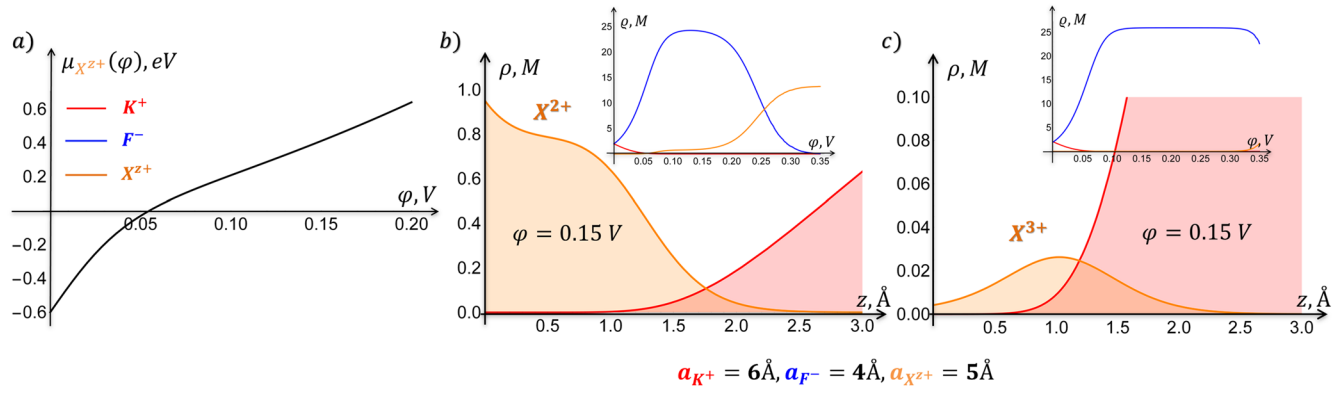

FIG. 11. A quasi-Faradaic process: the emergence of new charged species at the interface (metal dissolution). (a) The chemical potential of species X^{z+} as a function of the electrode potential $\mu_{X^{z+}}(\varphi)$. Only positive potentials are considered. [(b) and (c)] Ion density profiles near the electrode at φ = 0.15 eV for a model 2M KF solution when the emerging ions are X^{2+} and X^{3+}, respectively. The sizes of ions are 6 Å, 4 Å, and 5 Å for cations, anions, and X^{z+} species, respectively. The insets show the "polarization curves" for species.

For the sake of simplicity, here we consider a binary 1:1 2M solution with ions sizes set as 6 Å and 4 Å for cations and anions, respectively, and neglect all specific interactions by setting $\Phi_X = 0$. Moreover, we omit the spatial dependence of the dielectric function thus assuming $\varepsilon(z) = 80$. Our representative (phenomenological) chemical potential $\mu_{X^{z+}}(\varphi)$ is shown in Fig. 11(a). Its functional form guarantees that at $\varphi = 0$, the population of species X^{z+} is zero and ions X^{z+} are produced only at sufficiently positive potentials. The effective ion size of X^{z+} is set as 5 Å. In Figs. 11(b) and 11(c), we compare the ion density profiles of species X^{2+} and X^{3+} at the electrode potential $\varphi = 0.15$ V (the profile of anions is beyond this scale). The much smaller population of X^{3+} species can be understood in two ways. The insets show the "polarization curves" for these two cases. X^{2+} ions start dominating over the anions at potentials $\varphi > 0.25$ V, whereas X^{3+} ions dominate at much higher positive potentials. The electrostatic repulsion between the positively charged electrode ($\sigma \approx 56\ \mu C/cm^2$) and the ions X^{z+} makes the interfacial layers less populated with X^{3+} than with X^{2+} ions. This difference can potentially be used to discern relative populations of metal ions if electrochemical metal dissolution produces multiple ion types with distinct oxidation states. A similar approach can be used to simulate electrochemical reactions when new species emerge at the interface.

IV. CONCLUSION

In this work, we present a thermodynamic continuum model of electrified interfaces, based on a free energy functional with inclusion of electrostatic interactions with an idealized electrode and entropic considerations related to volume exclusion from a lattice gas model. Our formalism enables the description of multicomponent electrolytes, including the effects of specific adsorption, ion size disparity, and the explicit presence of neutral species. We disclose the generic role of the single-particle specific adsorption potential that bridges the microscopic and macroscopic description of the interface and show its effects on macroscopic descriptors, including the surface coverage and adsorption isotherms. The self-consistent procedure that we describe has the following advantages: It eliminates the need for *ad hoc* assumptions on the spatial characteristics of the Helmholtz compact layer; it describes the surface population in equilibrium with a bulk electrolyte of finite concentration, solely based on single particle descriptors; and consequently, it connects molecular-scale model parameters with thermodynamic observables. An additional feedback loop permits refining the model parameters by comparing with experimental data. There is an elegant duality to this approach that favors self-consistency between macroscopic and microscopic perspectives of the electrode/electrolyte interface: Inputs from minimal (i.e., tractable) AIMD simulations (without explicit consideration of finite concentration, for example) can be used to parameterize the continuum model; alternatively, the thermodynamic equilibrium presented by the continuum model and its associated expectation values for ion profiles or surface coverage at finite bias provide guidance for constructing realistic AIMD simulations consistent with thermodynamic boundary conditions. Future work will aim to develop hybrid AIMD-CM studies to explore larger time/length scale phenomenology of biased interfaces.

The general formalism that we present here not only provides access to the bias and concentration dependent equilibrium structure of the electrolyte in the vicinity of the interface but also provides estimates of the free energy costs associated with perturbation of the bulk structure of the electrolyte upon immersing a charged electrode with or without specific interactions with the electrolyte components. Since these estimates have a direct experimental counterpart in the surface tension, our model enables an additional experimental justification. Using the same approach, we could evaluate the relative probabilities of ion density fluctuations and thus the overall thermodynamic stability of the interface. This could help establish the requirements for the critical sizes of simulation cells that would exclude artifacts caused by insufficient number of species and/or unrealistic boundary conditions.

With little modification, we can consider the air/liquid or liquid/liquid interfaces and explore the spatial profiles of ions and their contribution to the liquid surface tension. In particular, it is intriguing to identify the factors that may lead to the non-monotonic dependence of the water surface tension as a function of the bulk concentration of ions or, more generally, find the parameters that could give rise to multiple minima in the free energy landscape of the interface. This could be important for the design of interfaces with a desired functionality.

The model can also be easily upgraded to include additional mechanisms of equilibration on top of the optimization of electrostatic, steric, and specific ion-electrode interactions. In this respect, we show how the local inhomogeneity of the spatial profile of ions near the interface can drive the system to a new equilibrium state when chemical transformations are accounted for. This functionality provides a sound basis for establishing the concept of local pH and shows the importance of interfacial speciation in contrast to the speciation in the bulk electrolyte. We show that local chemical composition can be significantly shifted as compared to the bulk and minor species may become dominant at the interface. We also show that the model can be extended to the case when the electrode acts as a reservoir of certain species and their chemical potential is controlled by the electrode potential (as in electrochemical dissolution of metal electrodes). With assumptions on the time scale of the potential-driven production of new species and their diffusion, our model helps to evaluate density profiles of new species depending on their state of charge, size, etc.

With the flexibility and the ease that different aspects can be combined and replaced, we believe that our model provides sufficient power to create a hybrid AIMD-CM self-consistent methodology for modeling electrified interfaces.

ACKNOWLEDGMENTS

This work was supported by the Joint Center for Energy Storage Research, an Energy Innovation Hub funded by the U.S. Department of Energy, Office of Science, Basic Energy Sciences. Portions of this work were supported by a user project at the Molecular Foundry and its compute cluster (vulcan), managed by the High Performance Computing Services Group, at Lawrence Berkeley National Laboratory (LBNL), and portions of this work used the computing resources of the National Energy Research Scientific Computing Center, LBNL, both of which are supported by the Office of Science of the U.S. Department of Energy under Contract No. DE-AC02-05CH11231. The authors thank Dr. Ph. Ross for useful discussions.

The authors declare no competing financial interest.

REFERENCES

[1] S. Nemšák, A. Shavorskiy, O. Karslioglu, I. Zegkinoglou, A. Rattanachata, C. S. Conlon, A. Keqi, P. K. Greene, E. C. Burks, F. Salmassi, E. M. Gullikson, S.-H. Yang, K. Liu, H. Bluhm, and C. S. Fadley, Nat. Commun. **5**, 5441 (2014).
[2] O. Karslioğlu, S. Nemšák, I. Zegkinoglou, A. Shavorskiy, M. Hartl, F. Salmassi, E. M. Gullikson, M. L. Ng, C. Rameshan, B. Rude, D. Bianculli, A. A. Cordones, S. Axnanda, E. J. Crumlin, P. N. Ross, C. M. Schneider, Z. Hussain, Z. Liu, C. S. Fadley, and H. Bluhm, Faraday Discuss. **180**, 35 (2015).
[3] M. Favaro, B. Jeong, P. N. Ross, J. Yano, Z. Hussain, Z. Liu, and E. J. Crumlin, Nat. Commun. **7**, 12695 (2016).
[4] J.-J. Velasco-Velez, C. H. Wu, T. A. Pascal, L. F. Wan, J. Guo, D. Prendergast, and M. Salmeron, Science **346**, 831 (2014).
[5] A. J. Bard and L. Faulkner, *Electrochemical Methods: Fundamentals and Applications* (Wiley, 1980).
[6] J. Newman and K. E. Thomas-Alyea, *Electrochemical Systems*, 3rd ed. (Wiley, 2004).
[7] J. Li, C. L. Fisher, J. L. Chen, D. Bashford, and L. Noodleman, Inorg. Chem. **35**, 4694 (1996).
[8] P. Winget, E. J. Weber, C. J. Cramer, and D. G. Truhlar, Phys. Chem. Chem. Phys. **2**, 1231 (2000).
[9] C. P. Kelly, C. J. Cramer, and D. G. Truhlar, J. Phys. Chem. B **110**, 16066 (2006).
[10] C. P. Kelly, C. J. Cramer, and D. G. Truhlar, J. Phys. Chem. B **111**, 408 (2007).
[11] V. S. Bryantsev, M. S. Diallo, and W. A. Goddard III, J. Phys. Chem. **112**, 9709 (2008).
[12] A. V. Marenich, J. Ho, M. L. Coote, C. J. Cramer, and D. G. Truhlar, Phys. Chem. Chem. Phys. **16**, 15068 (2014).
[13] D. C. Grahame and B. A. Soderberg, J. Chem. Phys. **22**, 449 (1954).
[14] R. Parsons, Trans. Faraday Soc. **55**, 999 (1959).
[15] E. Dutkiewicz and R. Parsons, J. Electroanal. Chem. **11**, 100 (1966).
[16] M. J. Weaver and F. C. Anson, J. Electroanal. Chem. **84**, 47 (1977).
[17] B. A. Pethica, Phys. Chem. Chem. Phys. **9**, 6253 (2007).
[18] E. Spohr, in *Advances in Electrochemical Science and Engineering, Volume 6* (Wiley, 1999), pp. 1–75.
[19] E. Spohr, Solid State Ionics **150**, 1 (2002).
[20] M. Otani and O. Sugino, Phys. Rev. B **73**, 115407 (2006).
[21] W. Schmickler, "Electrical double layers: Theory and simulations," in *Encyclopedia of Electrochemistry* (Wiley, 2007).
[22] R. Jinnouchi and A. B. Anderson, Phys. Rev. B **77**, 245417 (2008).
[23] J. Rossmeisl, E. Skúlason, M. E. Björketun, V. Tripkovic, and J. K. Nørskov, Chem. Phys. Lett. **466**, 68 (2008).
[24] E. Skúlason, V. Tripkovic, M. E. Björketun, S. Gudmundsdottir, G. Karlberg, J. Rossmeisl, T. Bligaard, H. Jnsson, and J. K. Nørskov, J. Phys. Chem. C **114**, 18182 (2010).
[25] V. Tripkovic, M. E. Björketun, E. Skúlason, and J. Rossmeisl, Phys. Rev. B **84**, 115452 (2011).
[26] M. E. Björketun, Z. Zeng, R. Ahmed, V. Tripkovic, K. S. Thygesen, and J. Rossmeisl, Chem. Phys. Lett. **555**, 145 (2013).
[27] N. Bonnet, I. Dabo, and N. Marzari, Electrochim. Acta **121**, 210 (2014).
[28] M. Nielsen, M. E. Björketun, M. H. Hansen, and J. Rossmeisl, Surf. Sci. **631**, 2 (2015).
[29] J. K. Nørskov, J. Rossmeisl, A. Logadottir, L. Lindqvist, J. R. Kitchin, T. Bligaard, and H. Jónsson, J. Phys. Chem. B **108**, 17886 (2004).
[30] S. Trasatti, J. Electroanal. Chem. **52**, 313 (1974).
[31] S. P. Ong, O. Andreussi, Y. Wu, N. Marzari, and G. Ceder, Chem. Mater. **23**, 2979 (2011).
[32] Y. Ando, Y. Kawamura, T. Ikeshoji, and M. Otani, Chem. Phys. Lett. **612**, 240 (2014).
[33] L. E. Camacho-Forero, T. W. Smith, S. Bertolini, and P. B. Balbuena, J. Phys. Chem. C **119**, 26828 (2015).
[34] P. Canepa, G. Sai Gautam, D. C. Hannah, R. Malik, M. Liu, K. G. Gallagher, K. A. Persson, and G. Ceder, Chem. Rev. **117**, 4287 (2017).
[35] K. Leung and C. M. Tenney, J. Phys. Chem. C **117**, 24224 (2013).
[36] K. Leung, Phys. Chem. Chem. Phys. **17**, 1637 (2015).
[37] K. Leung and A. Leenheer, J. Phys. Chem. C **119**, 10234 (2015).
[38] I. Tavernelli, R. Vuilleumier, and M. Sprik, Phys. Rev. Lett. **88**, 213002 (2002).
[39] R. Sundararaman, W. A. Goddard, and T. A. Arias, J. Chem. Phys. **146**, 114104 (2017).
[40] O. Sugino, I. Hamada, M. Otani, Y. Morikawa, T. Ikeshoji, and Y. Okamoto, Surf. Sci. **601**, 5237 (2007).
[41] N. Bonnet, T. Morishita, O. Sugino, and M. Otani, Phys. Rev. Lett. **109**, 266101 (2012).
[42] I. Rungger, X. Chen, U. Schwingenschlögl, and S. Sanvito, Phys. Rev. B **81**, 235407 (2010).
[43] A. Roldan, Curr. Opin. Electrochem. **10**, 1 (2018).
[44] R. Kubo, *Statistical Mechanics* (North-Holland Publishing Company, Amsterdam, 1965).
[45] N. Bonnet, O. Sugino, and M. Otani, J. Chem. Phys. **140**, 044703 (2014).
[46] C. Perego, M. Salvalaglio, and M. Parrinello, J. Chem. Phys. **142**, 144113 (2015).
[47] E. Anglada, J. Junquera, and J. M. Soler, Phys. Rev. E **68**, 055701(R) (2003).
[48] A. Glielmo, P. Sollich, and A. De Vita, Phys. Rev. B **95**, 214302 (2017).
[49] M. Vossen and F. Forstmann, J. Chem. Phys. **101**, 2379 (1994).
[50] A. Krämer, M. Vossen, and F. Forstmann, J. Chem. Phys. **106**, 2792 (1997).
[51] I. Borukhov, D. Andelman, and H. Orland, Phys. Rev. Lett. **79**, 435 (1997).
[52] I. Borukhov, D. Andelman, and H. Orland, Electrochim. Acta **46**, 221 (2000).
[53] A. Abrashkin, D. Andelman, and H. Orland, Phys. Rev. Lett. **99**, 077801 (2007).
[54] M. S. Kilic, M. Z. Bazant, and A. Ajdari, Phys. Rev. E **75**, 021503 (2007).
[55] Y.-H. Fang, G.-F. Wei, and Z.-P. Liu, Catal. Today **202**, 98 (2013).
[56] M. Z. Bazant, M. S. Kilic, B. D. Storey, and A. Ajdari, Adv. Colloid Interface Sci. **152**, 48 (2009).
[57] G. Fisicaro, L. Genovese, O. Andreussi, N. Marzari, and S. Goedecker, J. Chem. Phys. **144**, 014103 (2016).
[58] S. Ringe, H. Oberhofer, C. Hille, S. Matera, and K. Reuter, J. Chem. Theory Comput. **12**, 4052 (2016).
[59] N. Luque, S. Woelki, D. Henderson, and W. Schmickler, Electrochim. Acta **56**, 7298 (2011).
[60] S. Nishihara and M. Otani, Phys. Rev. B **96**, 115429 (2017).
[61] N. D. Mermin, Phys. Rev. **137**, A1441 (1965).
[62] Y. Rosenfeld and N. W. Ashcroft, Phys. Rev. A **20**, 1208 (1979).
[63] R. Evans, Adv. Phys. **28**, 143 (1979).
[64] J. P. Hansen and I. R. McDonald, *Theory of Simple Liquids*, 2nd ed. (Academic Press, London, 1986).
[65] R. Roth, J. Phys.: Condens. Matter **22**, 063102 (2010).
[66] P. Tarazona and R. Evans, Mol. Phys. **52**, 847 (1984).

[67]J. Forsman, C. E. Woodward, and R. Szparaga, *Computational Electrostatics for Biological Applications* (Springer, 2015), pp. 17–38.
[68]D. Henderson, L. Blum, and J. L. Lebowitz, J. Electroanal. Chem. **102**, 315 (1979).
[69]D. F. Calef and P. G. Wolynes, J. Phys. Chem. **87**, 3387 (1983).
[70]T. Biben, J. P. Hansen, and Y. Rosenfeld, Phys. Rev. E **57**, R3727 (1998).
[71]B. C. Freasier and S. Nordholm, J. Chem. Phys. **79**, 4431 (1983).
[72]A. Härtel, J. Phys.: Condens. Matter **29**, 423002 (2017).
[73]N. Georgi, A. Kornyshev, and M. Fedorov, J. Electroanal. Chem. **649**, 261 (2010).
[74]M. Ma, S. Zhao, and Z. Xu, Commun. Comput. Phys. **20**, 441 (2016).
[75]R. Wang and Z.-G. Wang, Phys. Rev. Lett. **112**, 136101 (2014).
[76]R. Wang and Z.-G. Wang, J. Chem. Phys. **142**, 104705 (2015).
[77]K. Letchworth-Weaver and T. A. Arias, Phys. Rev. B **86**, 075140 (2012).
[78]D. Gunceler, K. Letchworth-Weaver, R. Sundararaman, K. A. Schwarz, and T. A. Arias, Modell. Simul. Mater. Sci. Eng. **21**, 074005 (2013).
[79]R. Sundararaman, K. Letchworth-Weaver, and K. A. Schwarz, J. Chem. Phys. **148**, 144105 (2018).
[80]A. Kornyshev and M. Vorotyntsev, Surf. Sci. **101**, 23 (1980).
[81]F. Booth, J. Chem. Phys. **19**, 391 (1951).
[82]J. E. Curry and D. A. McQuarrie, Langmuir **8**, 1026 (1992).
[83]J.-L. Fattebert and F. Gygi, Int. J. Quantum Chem. **93**, 139 (2003).
[84]A. A. Kornyshev, J. Phys. Chem. B **111**, 5545 (2007).
[85]M. V. Fedorov and A. A. Kornyshev, Electrochim. Acta **53**, 6835 (2008).
[86]J. P. Valleau and G. M. Torrie, J. Chem. Phys. **76**, 4623 (1982).
[87]J. P. Valleau and G. M. Torrie, J. Chem. Phys. **81**, 6291 (1984).
[88]E. Gongadze, V. Kralj-Igli, and A. Igli, Gen. Physiol. Biophys. **36**, 229 (2017).
[89]Y.-X. Yu and J. Wu, J. Chem. Phys. **117**, 2368 (2002).
[90]D.-e. Jiang, D. Meng, and J. Wu, Chem. Phys. Lett. **504**, 153 (2011).
[91]J. Bikerman, Philos. Mag. **33**, 384 (1942).
[92]E. Wicke and M. Eigen, Z. Naturforsch., A: Phys. Sci. **8**, 161 (1953).
[93]A. Baskin and D. Prendergast, J. Electrochem. Soc. **164**, E3438 (2017).
[94]M. L. Foresti, M. Innocenti, F. Forni, and R. Guidelli, Langmuir **14**, 7008 (1998).
[95]L. Falciola, P. R. Mussini, S. Trasatti, and L. M. Doubova, J. Electroanal. Chem. **593**, 185 (2006).
[96]V. Marichev, Chem. Phys. Lett. **411**, 434 (2005).
[97]D. Larkin, K. L. Guyer, J. T. Hupp, and M. J. Weaver, J. Electroanal. Chem. Interfacial Electrochem. **138**, 401 (1982).
[98]G. Jones and W. A. Ray, J. Am. Chem. Soc. **59**, 187 (1937).
[99]M. D. Baer, I.-F. W. Kuo, D. J. Tobias, and C. J. Mundy, J. Phys. Chem. B **118**, 8364 (2014).
[100]T. Duignan, M. Baer, and C. Mundy, J. Chem. Phys. **149**, 194702 (2018).
[101]A. N. Frumkin, *Kinetics of Electrode Processes* (Moscow State University Press, 1952) (in Russian).
[102]A. N. Frumkin, Trans. Faraday Soc. **55**, 156 (1959).
[103]C. Nguyen Van Huong, C. Hinnen, and A. Rousseau, J. Electroanal. Chem. **151**, 149 (1983).
[104]A. W. Adamson and A. P. Gast, *Physical Chemistry of Surfaces* (Wiley, 1997).
[105]I. Gyarmati, *Non-Equilibrium Thermodynamics* (Springer-Verlag, Berlin, Heidelberg, New York, 1970).
[106]E. T. Jaynes, Ann. Rev. Phys. Chem. **31**, 579 (1980).
[107]R. Balescu, *Equilibrium and Nonequilibrium Statistical Mechanics* (John Wiley and Sons, 1975).